Unveiling plant tolerance mechanisms through a model coupling plant physiology and nematode epidemiology

Joseph Penlap Tamagoua[1,2,*], Suzanne Touzeau[1,2], Frédéric Grognard[1], and Valentina Baldazzi[1,2]

[1]Université Côte d'Azur, Inria, INRAE, CNRS, MACBES, France
[2]Université Côte d'Azur, INRAE, ISA, France
[*]Corresponding author: joseph.penlap@inria.fr

Abstract

Root-knot nematodes (RKN) of the genus *Meloidogyne spp.* cause considerable yield losses in numerous crops worldwide. Their name comes from the galls (root knots) they induce on the roots of their host during the establishment of their feeding site that enables nematodes to hijack plant resources. Plant reaction to parasitism by RKN strongly depends on the plant species and cultivar. This study focuses on tolerant plants, which are plants able to cope with nematode infections with limited yield losses. We aim at identifying the mechanisms underlying plant tolerance through an original model of plant–RKN interactions.

We built an original mechanistic model of plant–RKN interactions that explicitly links plant physiology and pest demography. The model represents both the free-living and within-root dynamics of RKN, the latter depending on plant resources. On the plant side, it differentiates the root, shoot and fruit compartments and it takes into account the carbon and water resources, that are altered by nematode infection. We calibrated the model on experimental data of two annual horticultural crops: tomato and pepper, the latter being considered more tolerant to nematode infection. We compared both plants to get insights on parameters and traits that could explain their different tolerance levels.

The calibration results show a good fit to the experimental data for both species, capturing growth trends and infection dynamics. Nematode damage was greater in tomato than in pepper, with higher gall severity observed in tomato. Early fruiting in pepper limited resource diversion to nematodes, preserving yield while allowing moderate nematode populations. Virtual tomato experiments revealed that tolerance arises from a combination of traits: high resource acquisition, vigorous root and shoot growth, and a robust carbon allocation towards fruits, which individually or synergistically mitigate the effects of RKN parasitism. Moreover, these traits remained robust across different RKN virulence scenarios.

Keywords: Root-knot nematodes, plant physiology, dynamical systems, sensitivity analysis.

Contents

1 Introduction

Root-knot nematodes (RKN), of the genus *Meloidogyne spp.*, are microscopic roundworms that are among the most devastating plant-parasitic nematodes worldwide. These obligate endoparasites infect a broad host range of commercially important crop families such as the *Solanaceae* (pepper, potato, tomato), *Fabaceae* (soybean), *Malvaceae* (cotton), *Amaranthaceae* (sugar beet), and *Poaceae* (maize, wheat, rice) (Sato et al., 2019). Typical symptoms include stunted growth, wilting, chlorosis, and reduced fruiting, which reduce both yield and produce quality (Downton, 1977; Wilkes and Kirkpatrick, 2020; Mu and Chen, 2021). RKN feed on plant roots, causing the formation of galls or knots that disrupt normal root architecture. This makes plants more susceptible to drought stress and reduces nutrient uptake efficiency (Williamson and Hussey, 1996; Jammes et al., 2005), often increasing vulnerability to other soilborne pathogens (Jones et al., 2013).

The economic impact of RKN is substantial, with crop losses estimated in the billions of dollars annually (Ralmi et al., 2016; Subbotin et al., 2021), highlighting the global threat they pose to food security and agricultural profitability. Losses are particularly severe in African countries, where farming conditions may be suboptimal (Ajayi, 2020). For instance, in tropical vegetable crops, yield reductions range from 17-20% in eggplant, 18-33% in melon, and 24-38% in tomato (Sasser, 1979). Another study reported that RKN can decrease crop yields by 2-45%, depending on the crop and infestation severity (Anwar and Mckenry, 2012).

Plant species differ markedly in their responses to nematode parasitism and are generally classified as susceptible, resistant, or tolerant. Susceptible plants are highly vulnerable to nematode attacks, often suffering substantial yield losses. Resistant plants, whether qualitative or quantitative, possess specific genetic mechanisms that inhibit or block nematode development (Cook et al., 1997; Tomczak et al., 2009), typically through pattern-recognition receptors that activate defense responses (Sato et al., 2019). Only a limited number of resistance genes have been identified, so far, though, and only in horticultural crop species, including tomato (*Mi-1*), pepper (*Me1*, *Me3*), soybean (*Rhg1*, *Rhg4*), and potato (*H1*) (Ornat et al., 2001; Djian-Caporalino et al., 2007; Cook et al., 2012; Pineda et al., 1993). Moreover, experiments have shown that prolonged used of resistance plants can lead to the emergence of virulent nematodes thus reducing its long-term efficacy (Meher et al., 2009; Djian-Caporalino et al., 2011).

Between these two extremes lie tolerant plants, which have the ability to withstand nematode infection with minimal impact on yield (Cook et al., 1997). Quantitative resistance blocks pathogen multiplication, whereas tolerance mitigates the damage caused by infection without restricting nematode development, which can pose epidemiological risks for subsequent crops (Bishop, 2012; Barbary et al., 2015). Within the Solanaceae family, pepper is generally considered more tolerant than tomato to RKN (Castagnone-Sereno et al., 1992), making it a valuable option in crop rotations or under high nematode pressure (Mekete et al., 2003; Hallmann and Meressa, 2018).

Unlike resistance, tolerance is not always considered from a strictly genetic perspective, as it may involve a variety of phenotypic mechanisms (Ney et al., 2013). Consequently, the mechanisms underlying tolerance remain difficult to characterize, likely reflecting a wide range of physical, molecular, and physiological traits that, alone or in combination, enable plants to mitigate or compensate for nematode-induced damage while maintaining essential functions for growth and reproduction (Wallace, 1987; Wise and Abrahamson, 2005; Ney et al., 2013).

Better understanding the mechanisms underlying tolerance is a key challenge for nematode management as it can lead to the selection of new crop varieties that are more resilient. Mechanistic modelling provides valuable tools to integrate biological knowledge, quantify system dynamics, and support the design of sustainable control strategies. Many existing models address plant–pest dynamics; however, most either focus solely on the pest or the plant, overlooking their interactions, or they simplify essential physiological and epidemiological processes, thereby limiting their practical relevance (Aggarwal et al., 2006; Dietze and Matthes, 2014).

Several epidemiological models have been proposed to study the dynamics of soilborne pests and their impacts on host growth. In most cases, the infection dynamics are restricted to root-level processes without explicitly accounting for plant physiology. For example, Cunniffe and Gilligan (2011) developed a theoretical model to explore various strategies for managing soilborne fungal pathogens. Tankam-Chedjou et al. (2020) developed a semi-discrete model of banana and plantain infestation by *R. similis* with limited host–pathogen coupling, and Nilusmas et al. (2020) proposed an epidemiological model describing avirulent and virulent RKN dynamics to optimize resistance deployment. Similarly, Yadav and Kumar (2022) built a prey–predator model for banana–nematode interactions but oversimplified host physiology. Such models mainly describe pest populations and their effects on hosts, without incorporating host responses or environmental factors.

Plant growth models such as *STICS* (Brisson et al., 2003), *DSSAT* (Jones et al., 2003), *AquaCrop* (Steduto et al., 2009), and *CropSyst* (Stöckle et al., 2003) are simulation-based that describe how plants grow and develop over time under various environmental, genetic, and management conditions. However, plant parasitism is rarely considered in these models, despite being a key factor for agronomic, ecological, and economic sustainability (Kropff et al., 1995). For example, in *SIMBA-NEM* model (Tixier et al., 2006), which simulated the population dynamics of two major plant-parasitic nematode species of banana *Radopholus similis* and *Pratylenchus coffeae*, a simple logistic function was used to represent pest population growth. In most cases, pest dynamics are incorporated only as a single growth function or as exogenous stress factors and neglect the developmental biology of the parasites.

There is a clear need for models that explicitly integrate both epidemiological and ecophysiological perspectives to capture the complexity of plant–nematode interactions. A notable attempt is the framework of Zaffaroni et al. (2020), who integrated aphid population dynamics with plant growth. This coupled approach allowed for a more dynamic understanding of how pest populations affect plant development and how plants defend themselves. However, there are some modifications that need to be made for its adaptation to RKN systems. For instance, the aphid in their model is an airborne pest, whereas RKN are soilborne, which introduces different ecological dynamics, particularly in how nematodes interact with the root system. Additionally, their study was focused only on the plant vegetative stage, whereas RKN infestations also affect the reproductive stage, which could be crucial to better quantify the damage and assess plant

productivity. More recently, Penlap Tamagoua et al. (2025) developed a generic model linking plant and nematode development through resource allocation. While their framework can accommodate most soilborne parasites, the representation of plant growth requires greater detail to capture distinct developmental stages.

The objective of this study is to elucidate the physiological mechanisms underlying plant tolerance to RKN infestation in horticultural crops. To this end, we: (i) develop a mechanistic model that captures the interplay between plant physiology and RKN population dynamics. RKN infestation disrupts plant physiology by depleting plant resources, and the plant physiological status influences the success and development of the RKN population; (ii) calibrate the model using experimental data from tomato and pepper, two species with contrasting tolerance levels; (iii) compare the parameter values and dynamical patterns of both species, to identify candidate mechanisms of tolerance.

This paper is organized as follows: Section 2 is devoted to the formulation of a mechanistic model of plant–nematode interactions based on plant physiology and nematode life cycle. Section 3 covers the materials and methods used to calibrate the model. Experimental data are described in Section 3.1, and the calibration procedure in Section 3.2. Section 4 presents the calibration results for healthy and infested plants, compares tomato and pepper parameters, identifies tolerance-related traits, and tests their robustness under different epidemiological scenarios. Section 5 concludes with a discussion on the dynamical patterns of the two species, providing insights on the plant tolerance mechanisms and discussing the impacts of nematode infestation on plant health.

2 Modelling plant–RKN interactions

Our dynamical model, coupling plant physiology and nematode demography is illustrated in Figure 1. We first describe the healthy plant model in Section 2.1. Then we present the RKN dynamics and their interactions with the plant in Section 2.2.

2.1 Healthy plant model

The plant model is based on the transport-resistance formalism, introduced by Thornley in the late 70s (Thornley, 1972; Thornley and Johnson, 1990). Accordingly, the plant is described as a collection of compartments, sharing essential resources via a resistive transport network. With respect to the original models, which focus on the vegetative phase, we added a fruit compartment as an additional and competitive carbon sink for plant.

Plant growth is described through the assimilation and allocation of two main resources : carbon and water. Carbon is acquired by shoots via photosynthesis and is converted in structural biomass within the plant. Water is absorbed by the roots and follows an upward circulation to supply the different plant compartments. We decided not to include nitrogen, since it does not influence nematode infestation (Spiegel et al., 1982).

Carbon transport from shoots to roots and fruits is modeled following the approach of Minchin et al. (1993), who explored a mechanistic 1-source 2-sink model of phloem transport. to explain the concept of sink priority. Water transport is described following an electric analogy, based on compartment-specific water potentials and hydraulic resistances between compartments (Dewar,

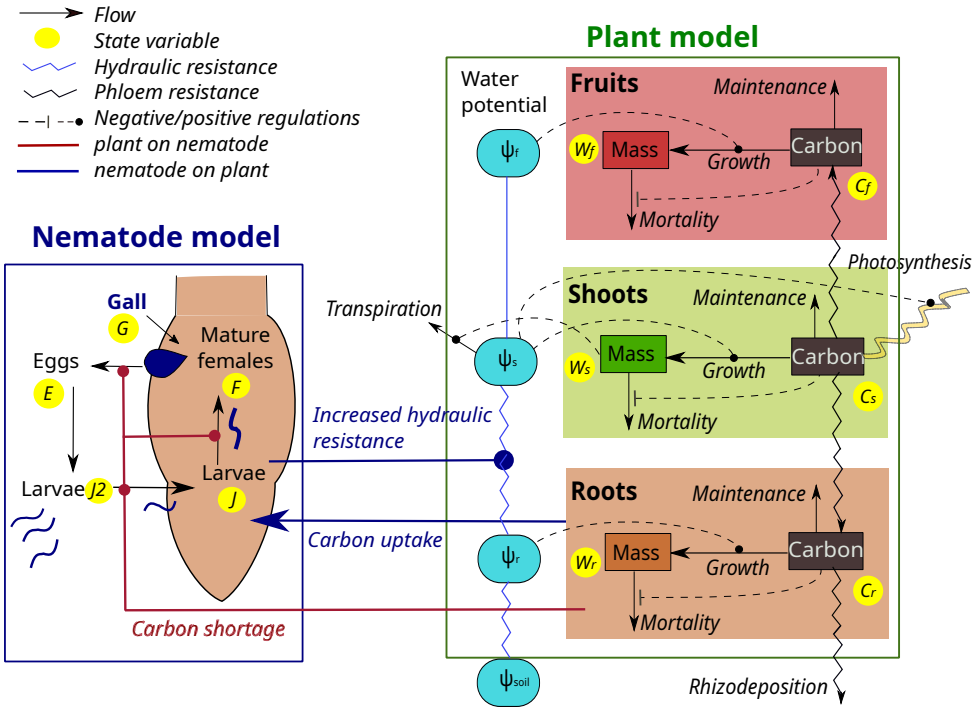

Figure 1: Scheme of the plant–nematode interaction model: root-knot nematode dynamics (left side) and plant dynamics (right side). **Nematodes**. Their life cycle is summarised in four stages: eggs (E) hatch and become juvenile larvae (J_2) in the soil; they enter the roots and become infesting larvae (J); they induce gall formation and mature into females (F), which lay eggs outside the roots. **Plant**. It is subdivided in three compartments: shoots (index s), roots (index r), and fruits (index f). Each compartment is characterised by its structural dry mass (W), carbon concentration (C) and water potential (ψ). Two resources are considered: carbon and water. Carbon uptake occurs in the shoots through photosynthesis, is transported using a transport-resistance model, and is released in the soil through rhizodeposition. Carbon is used for growth and maintenance. Water transport from the soil is driven by leaf transpiration and based on water potentials. **Interactions**. Nematodes in the roots divert carbon for their development and galls increase root hydraulic resistance (dark blue). Carbon shortage in the roots reduces egg laying, larvae establishment and triggers male development (dark red). Phloem (carbon transport) and hydraulic resistances decrease with the dry masses of the connected compartments (not represented); we assume that there is no resistance between shoots and fruits ($\psi_f = \psi_s$).

1993; Thornley, 1996). Interactions between water status and plant processes are described by threshold-dependent regulatory function of the water potential.

2.1.1 Plant model equations

Based on the choices presented above, we obtained a plant model structured in three compartments: shoots (index s), roots (index r) and fruits (index f). The model, depicted in Figure 1, describes the dynamics of the structural dry mass W_x and carbon concentration C_x in each compartment ($x = s, r, f$), as shown in the following equations:

$$
\begin{cases}
\text{Shoot} \begin{cases}
\dfrac{dW_s}{dt} = \underbrace{k_s\, f_k(\psi_s)\, \dfrac{C_s}{K_s + C_s}\, W_s}_{\text{Growth}} - \underbrace{d_s \left(1 + \dfrac{K_m^n}{K_m^n + C_s^n}\right) W_s}_{\text{Mortality}}, \\
\dfrac{dC_s}{dt} = \underbrace{p\, \dfrac{K_u}{K_u + W_s} f_p(\psi_s)}_{\text{Uptake}} - \underbrace{\dfrac{1}{W_s}\,(T_r + T_f + T_a)}_{\text{Transport}} - \underbrace{c\,(k_s + v_s)\, f_k(\psi_s) \dfrac{C_s}{K_s + C_s}}_{\text{Growth+Respiration}} - \underbrace{m_s\, \dfrac{C_s^n}{K_m^n + C_s^n}}_{\text{Maintenance}} - \underbrace{\dfrac{1}{W_s} \dfrac{dW_s}{dt} C_s}_{\text{Dilution}},
\end{cases} \\
\text{Root} \begin{cases}
\dfrac{dW_r}{dt} = \underbrace{k_r\, f_k(\psi_r)\, \dfrac{C_r}{K_r + C_r}\, W_r}_{\text{Growth}} - \underbrace{d_r \left(1 + \dfrac{K_m^n}{K_m^n + C_r^n}\right) W_r}_{\text{Mortality}}, \\
\dfrac{dC_r}{dt} = \underbrace{\dfrac{1}{W_r} T_r}_{\text{Transport}} - \underbrace{c\,(k_r + v_r)\, f_k(\psi_r) \dfrac{C_r}{K_r + C_r}}_{\text{Growth+Respiration}} - \underbrace{m_r\, \dfrac{C_r^n}{K_m^n + C_r^n}}_{\text{Maintenance}} - \underbrace{z\, C_r}_{\text{Rhizodeposition}} - \underbrace{\dfrac{1}{W_r} \dfrac{dW_r}{dt} C_r}_{\text{Dilution}},
\end{cases} \\
\text{Fruit} \begin{cases}
\dfrac{dW_f}{dt} = \underbrace{k_f\, f_k(\psi_f)\, \dfrac{C_f}{K_f + C_f}\, W_f}_{\text{Growth}} - \underbrace{d_f\, W_f}_{\text{Mortality}}, \\
\dfrac{dC_f}{dt} = \underbrace{\dfrac{1}{W_f}(T_f + T_a)}_{\text{Transport}} - \underbrace{c\,(k_f + v_f)\, f_k(\psi_f) \dfrac{C_f}{K_f + C_f}}_{\text{Growth+Respiration}} - \underbrace{m_f\, \dfrac{C_f^n}{K_m^n + C_f^n}}_{\text{Maintenance}} - \underbrace{\dfrac{1}{W_f} \dfrac{dW_f}{dt} C_f}_{\text{Dilution}}.
\end{cases}
\end{cases}
\tag{1}
$$

We describe below the processes that affect the healthy plant dynamics. Parameters are given in Table 1.

Water transport and stress: Water transport in the plant is driven by leaf transpiration and based on compartment-dependent water potentials ψ_x ($x = s, r, f$). We assume that the water potential of the soil ψ_{soil} is constant. The water potentials decrease from soil to shoots: the higher the hydraulic resistance, the higher the decrease. Hydraulic resistances are decreasing functions of the compartment dry masses. We assume that the resistance of aerial xylem vessels between shoots and fruits is negligible, so $\psi_f = \psi_s$. The dynamics of the root ψ_r and shoot ψ_s water potentials, together with the hydraulic resistance functions, are detailed in Section A.1. It leads to two additional dynamic equations for the plant model (13).

Processes such as growth (index g) and photosynthesis (index p) are affected by water stress, which occurs when the water potential ψ_x decreases below a process-dependent threshold value K_z (with $z = k, p$). To represent this effect, we introduce the following decreasing Hill functions:

$$
f_z(\psi_x) = \frac{K_z^n}{K_z^n + \psi_x^n}. \tag{2}
$$

We assume that growth is affected before photosynthesis, so $K_k > K_p$. The Hill coefficient n determines the steepness of the sigmoid.

Carbon uptake: Carbon uptake in the shoots occurs through photosynthesis. The carbon uptake per unit of shoot dry mass occurs at rate p and decreases when the dry mass increases, due to self-shading. Moreover, it is also reduced in case of water stress.

Carbon transport: Sap flows within phloem vessels along carbon concentration gradients, from shoots to roots and fruits. We use a transport-resistance model based on a 1-source 2-sink approach, as described in (Thornley and Johnson, 1990; Minchin et al., 1993). We assume that compartment-specific phloem resistances decrease with the compartment dry mass. We also consider an additional active carbon transport T_a from shoot to fruit for fruit ripening (Fishman and Génard, 1998; Liu et al., 2007). More details are provided in Section A.2.

Fruit onset: As the plant grows, fruits start to appear once the shoot dry mass reaches a threshold denoted W_{onset}, corresponding to plant maturity. This switch is modeled by the following Hill function:

$$M(W_s) = \left(\frac{W_s^n}{W_{\text{onset}}^n + W_s^n} \right). \tag{3}$$

The latter acts on transport allocation to roots or fruits as well as on the active transport Section A.2.

Growth: In each compartment, growth corresponds to the transformation of free carbon into structural biomass (c being the carbon fraction in structural dry matter). Growth follows a Michaelis-Menten kinetics with compartment-dependent saturation value k_x and threshold K_x (with $x = r, s, f$). During the growth process, part of the carbon used is lost through growth respiration at rate v_x. The maximum growth rate is reduced in case of water stress.

Maintenance: It corresponds to the carbon used to sustain the plant physiological activity, independently of growth processes. When carbon is abundant compared to threshold K_m, maintenance is constant at rate m_x. However when carbon becomes scarce compared to a threshold K_m, the maintenance is limited and plant mortality increases, in order to alleviate carbon shortage.

Mortality: Each dry mass compartment is affected by natural mortality at a basic rate d_x, that increases and can be doubled in case of carbon shortage.

Rhizodeposition: Plant roots release organic compounds into the soil. In particular, 5-10% of carbon fixed by photosynthesis is released (Barber and Martin, 1976). This process is introduced in the model, with a constant rate z.

Dilution: The dilution term in each carbon concentration equation is due to compartment growth.

The plant model, described in equations (1) and (13), was subjected to a series of abiotic tests to support its consistency with biological observations (see Section D.3).

Table 1: Plant model parameters for tomato and pepper: values are **estimated** (numeric exponents for range sources), set from data (†,‡ exponents) or from the literature (numeric exponents for sources). Parameters with identical values for tomato and pepper are only indicated once (in-between column).

Parameter	Description	Tomato		Pepper	Unit
		Value [range]		Value [range]	
p	**Photosynthesis rate**[3]	**0.144** [0.1–1]		**0.177** [0.1–1]	day^{-1}
σ_W	Shoot transpiration rate‡		13		day^{-1}
$r_{ph,x} = r_{ph}$	**Phloem resistance coefficients to carbon flow**^{*,3}	**0.131** [10^{-2}–0.5]		**0.0403** [10^{-2}–0.5]	$\text{g}^{\alpha-1} \cdot \text{day}$
$r_{xy,x} = r_{xy}$	Xylem resistance coefficient to water flow‡		4.9		$\text{g}^{\alpha-1} \cdot \text{day}$
r_{sr}	Resistance coefficient to water absorption by roots[7]		1		$\text{g}^{\alpha-1} \cdot \text{day}$
k_s, k_r, k_f	**Biomass growth rates**[3,8]	**0.211, 0.102, 0.967** $[0.1-1]$		**0.191, 0.103, 0.627** $[0.1-1]$	day^{-1}
K_s, K_r, K_f	Half-saturation constants for growth[3]	0.1, 0.01, 0.05		0.1, 0.01, 0.05	–
d_s, d_r, d_f	Mortality rates[3,6]	1/35, 1/75, 1/60		1/35, 1/200, 1/60	day^{-1}
ψ_{soil}	Water potential of soil$^{\diamond}$[,7]		-100		kPa
n	Hill coefficient$^{\diamond}$[,0]		6		–
W_{onset}	Threshold shoot biomass for fruit onset†	15		3	g
K_k	Half-saturation constant of the water effect on growth[1]	-1200		-1400	kPa
K_p	Half-saturation constant of the water effect on photosynthesis[1]	-1400		-1600	kPa
c	Carbon fraction of structural dry matter[2]		0.45		–
$\alpha_x = \alpha$	Allometric coefficients for growth†		0.63		–
$m_x = m$	Maintenance rates[3]		0.01		day^{-1}
$v_x = v$	Growth respiration rates[5]		0.035		day^{-1}
z	Rhizodeposition rate$^{\diamond}$[,7]		0.1		day^{-1}
K_m	Half-saturation constant for maintenance[3]		0.002		–
t_a	**Active transport rate**[4]	**0.207** [10^{-2}–0.5]		**0.298** [10^{-2}–0.5]	day^{-1}
K_u	Half-saturation constant for self-shading[0]	10		3	g
K_a	Half-saturation constant for active transport[4]		0.08		–
K_i	half-saturation constant for fruit carbon inhibition[0]		0.2		–

Note: $x = s, r, f$ (for shoots, roots, and fruits) indicated for compartment-independent values. $^{\star}r_{ph,s} = r_{ph,r} = \mathbf{2}\, r_{ph,s} = r_{ph}$. $^{\diamond}$fixed for the sensitivity analysis.

Sources for values/ranges: †estimated from data (Jauzion-Graverolle et al., 2025) and ‡computed in Section C.5.1; ^{0}assumed; ^{1}(Weng, 2000; Delfine et al., 2002); ^{2}(Li, 2007); ^{3}(Brugge, 1985); ^{4}(Liu et al., 2007); ^{5}(Thornley and Cannell, 2000); ^{6}(Wang et al., 2024); ^{7}(Dewar, 1993); ^{8}(Gerlin et al., 2022).

2.2 Coupled plant–nematode model

2.2.1 Nematode model

The pest population model is based on the RKN life cycle. In brief, adult females deposit eggs on the surface of the root. Infective J_2 larvae hatch in the soil, migrate towards suitable hosts and penetrate the root from the apex. Once inside the root, the RKN establish a feeding site and divert nutrients from the plant host. The larvae moult twice (J_3 and J_4 stages) until they become mature females, thus closing the cycle. Under unfavourable conditions, some of the larvae may develop into males, which eventually leave the root without contributing to RKN proliferation (Moens et al., 2009).

Accordingly, we distinguish four stages of nematode development in this model: eggs (E), juvenile larvae (J_2), infesting larvae (J), which include sedentary J_3 and J_4 stages and mature females (F). Males are not explicitly introduced in the model, as they affect neither pest reproduction nor plant growth, but their emergence is accounted for in the dynamics of the J larvae. The dynamics of the RKN population (left side of Figure 1) is described by the following equations:

$$
\begin{aligned}
\text{Free} \begin{cases} \dfrac{dE}{dt} = \underbrace{\rho(C_r)\,F}_{\text{Egg laying}} - \underbrace{\lambda\,E}_{\text{Hatching}} - \underbrace{\mu_E\,E}_{\text{Mortality}}\,, \\ \dfrac{dJ_2}{dt} = \underbrace{\lambda\,E}_{\text{Hatching}} - \underbrace{\beta\,J_2\,W_r}_{\text{Root entering}} - \underbrace{\mu_{J_2}\,J_2}_{\text{Mortality}}\,, \end{cases} \\
\text{In the root} \begin{cases} \dfrac{dJ}{dt} = \underbrace{\omega(C_r)\,\beta\,J_2\,W_r}_{\text{Root establishment}} - \underbrace{\eta\,J}_{\text{Maturation}} - \underbrace{\mu_J J}_{\text{Mortality}} - \underbrace{\nu(C_r)J}_{\text{Male development}}\,, \\ \dfrac{dF}{dt} = \underbrace{\eta\,J}_{\text{Maturation}} - \underbrace{\mu_F\,F}_{\text{Mortality}}\,. \end{cases}
\end{aligned}
\tag{4}
$$

Eggs hatch and become juvenile larvae at rate λ. These larvae enter root tips at infection rate β, but only a fraction $\omega(C_r)$ manages to establish its feeding site in the root, depending on the carbon availability. This fraction becomes infesting larvae, which develop into mature females after an average maturation period $\frac{1}{\eta}$. Females lay eggs at rate $\rho(C_r)$ which depends on carbon availability in the roots. All stages undergo stage-dependent natural mortality μ_Y (with $Y = E, J_2, J, F$). The development of larvae into males is represented by an additional carbon-dependent mortality rate $\nu(C_r)$ (Snyder et al., 2006). RKN parameters are described in Table 2. Plant impact on nematode dynamics, represented in dark red in Figure 1 and equations (4), is based on root carbon concentration C_r. Carbon shortage reduces egg laying, prevents larvae establishment and triggers male development. Corresponding equations, based on Hill functions, are illustrated in Figure 2 and given by:

$$
\rho(C_r) = \rho_{\min} + (\rho_{\max} - \rho_{\min}) \left(\frac{C_r^n}{K_\rho^n + C_r^n} \right), \quad \omega(C_r) = \left(\frac{C_r^n}{K_\omega^n + C_r^n} \right), \quad \nu(C_r) = \nu \left(\frac{K_\omega^n}{K_\omega^n + C_r^n} \right).
\tag{5}
$$

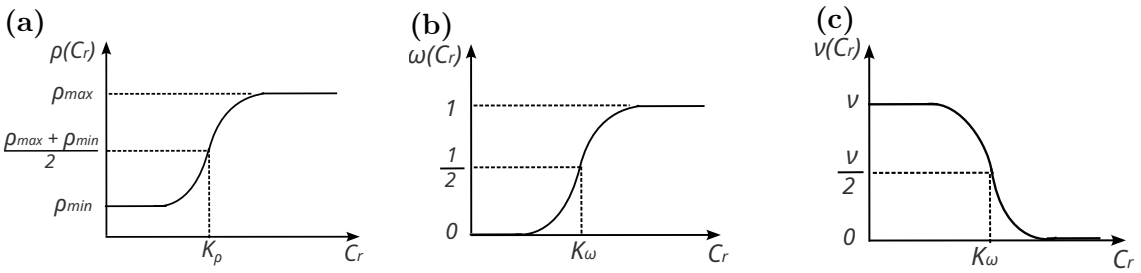

Figure 2: Influence of plant carbon availability on nematode development: (a) reproduction $\rho(C_r)$; (b) establishment $\omega(C_r)$; (c) male development $\nu(C_r)$.

2.2.2 Infested plant model

The presence of nematodes strongly affects plant physiology, introducing additional terms in equations (1). When nematodes successfully establish their feeding sites in roots, they create galls. Galls grow faster than healthy roots. So we chose to represent the dynamics of galls as a new variable W_g distinct from the healthy root biomass W_r:

$$
\begin{cases}
\dfrac{dW_r}{dt} = \underbrace{k_r f_k(\psi_r)\dfrac{C_r}{K_r + C_r} W_r}_{\text{Growth}} - \underbrace{d_r \left(1 + \dfrac{K_m^n}{K_m^n + C_r^n}\right) W_r}_{\text{Mortality}}, \underbrace{-\omega(C_r)\,\epsilon\,\beta\,J_2\,W_r}_{\text{Gall formation}}, \\
\dfrac{dW_g}{dt} = \underbrace{\omega(C_r)\,\epsilon\,\beta\,J_2\,W_r}_{\text{Gall formation}} + \underbrace{k_g f_k(\psi_r)\dfrac{C_r}{K_g + C_r} W_g}_{\text{Growth}} - \underbrace{d_r\,W_g}_{\text{Mortality}}, \\
\dfrac{dC_r}{dt} = \dfrac{1}{(W_r + W_g)} \underbrace{T_r}_{\text{Transport}} - \underbrace{\dfrac{c f_k(\psi_r)}{W_r + W_g}\left((k_r + v_r)\dfrac{C_r}{K_r + C_r} W_r + (k_g + v_r)\dfrac{C_r}{K_g + C_r} W_g\right)}_{\text{Growth + Respiration}} \\
\qquad - \underbrace{z\,C_r}_{\text{Rhizodeposition}} - \underbrace{m_r \left(\dfrac{C_r^n}{K_m^n + C_r^n}\right)}_{\text{Maintenance}} - \underbrace{\dfrac{C_r}{(W_r + W_g)}\left(\dfrac{dW_r}{dt} + \dfrac{dW_g}{dt}\right)}_{\text{Dilution}} \\
\qquad - \underbrace{\dfrac{1}{(W_r + W_g)}\gamma\left(\dfrac{C_r}{K_\gamma + C_r}\right)(J + F)}_{\text{Nematode feeding}}.
\end{cases}
\tag{6}
$$

Gall formation derives from successful nematode establishment in roots, described in equation (4), with conversion parameter ϵ, which gives the healthy root dry mass diverted by a nematode. Once initiated, galls follow the same dynamics as healthy roots but they have a higher growth rate k_g and a greater affinity for root carbon. Gall growth and nematode feeding act as additional carbon sinks for roots. Both J larvae and females are assumed to feed at a maximum rate γ, modulated by root carbon availability.

In the infested scenario, the main change in carbon concentration dynamics is that the total root biomass, W_r, without nematodes, becomes $W_r + W_g$ when nematodes are present. Note that higher root biomass $W_r + W_g$ results in higher phloem conductivity and more carbon transported from shoots to roots, in order to sustain nematode development. Additionally, the presence of galls has an impact on water transport (Dorhout, 1991). Xylem resistance is assumed to increase linearly with the gall density which progressively impairs the plant ability to retrieve water from the soil. More details can be found in Section A.1.

Table 2: RKN and interaction parameters for tomato and pepper: values are **estimated**, set from data (†,‡ exponents) or from the literature (numeric exponents for sources). Parameters with identical values for tomato and pepper are only indicated once (in-between column).

Parameter	Description	Tomato		Pepper	Unit
		Value [range]		Value [range]	
λ	Hatching rate‡		$0.46/13$		day^{-1}
η	Larva maturation rate[2]		$1/18$		day^{-1}
β	**Infection rate**	$\mathbf{1.06 \cdot 10^{-1}}$ [10^{-2}–0.2]		$\mathbf{6.04 \cdot 10^{-2}}$ [10^{-2}–0.2]	day^{-1}
ϵ	Infection conversion coefficient[3]		$5 \cdot 10^{-8}$		$\text{g} \cdot \text{ind}^{-1}$
γ	**Feeding rate**	$\mathbf{4.49 \cdot 10^{-6}}$ [10^{-7}–10^{-5}]		$\mathbf{2.04 \cdot 10^{-6}}$ [10^{-7}–10^{-5}]	day^{-1}
$\rho_{\min}$	Minimum egg laying rate†	$230 \cdot \mu_F$		$250 \cdot \mu_F$	day^{-1}
$\rho_{\max}$	Maximum egg laying rate†	$330 \cdot \mu_F$		$350 \cdot \mu_F$	day^{-1}
K_ρ	**Half-saturation constant for reproduction**	$\mathbf{8.93 \cdot 10^{-4}}$ [10^{-5}–10^{-3}]		$\mathbf{1.51 \cdot 10^{-4}}$ [10^{-5}–10^{-3}]	–
K_γ	Half-saturation constant for feeding	K_ρ		K_ρ	–
K_ω	**Half-saturation constant for establishment**	$K_\rho \times \mathbf{0.951}$ [0.1–1]		$K_\rho \times \mathbf{0.2}$ [0.1–1]	–
ν	Male production rate when carbon is scarce[4]		$1/4$		day^{-1}
μ_E	Mortality rate of eggs‡		$0.54/13$		day^{-1}
μ_{J_2}	Mortality rate of juvenile larvae[1]		$1/4$		day^{-1}
μ_J	Mortality rate of infesting larvae[1]		$1/13$		day^{-1}
μ_F	Mortality rate of mature females[1]		$1/13$		day^{-1}
k_g	**Gall growth rate**	**0.288** [0.1–1]		**0.31** [0.1–1]	day^{-1}
K_g	Half-saturation constant for gall formation	$K_r/10$		$K_r/10$	–
ϕ	Coefficient of gall impact on root xylem resistance†	8		2	day^{-1}

Sources for values/ranges: †estimated from data (Jauzion-Graverolle et al., 2025) and ‡computed in Section C.5.2; [1](Subedi et al., 2020); [2](Nilusmas et al., 2020); [3](Cabrera et al., 2015); [4](Snyder et al., 2006).

3 Materials and methods

We first describe the experimental data, then the model calibration based on these data, the initial conditions used for the model simulations, and finally some metrics used to display model outputs.

3.1 Experimental data

The study used data from an experiment conducted at INRAE in Sophia Antipolis (south of France) during spring 2021 Jauzion-Graverolle et al. (2025), for two Solanaceae species: tomato (*Solanum lycopersicum* cv. Saint Pierre) and pepper (*Capsicum annuum* cv. Doux Long des Landes). Thirty plants of each species were grown in a greenhouse, under standard culture conditions. At time zero, half of the plants were inoculated with 20,000 *Meloidogina incognita* eggs, after which plant growth and nematode development were monitored for 12 weeks, which corresponds to approximately two nematode life cycles.

Destructive measurements were taken initially and at two time points six weeks apart, with six replicates per crop (tomato or pepper), time point, and treatment (control/healthy vs infected plants), except at time zero when the six same replicates were used for both treatments (no nematode impact yet). Plant measurements included the dry mass of shoots (W_s), roots (W_r), and fruits (W_f) (Table 6), as well as the non destructive weekly monitoring of leaf number (L_f) (Table 5). Nematode data included the number of galls at the 6-week time point, as well as egg masses and eggs per egg mass at each time point. At the end of the experiment, the abundance of free-living larvae was estimated from contaminated soils (Table 7).

3.2 Model calibration

Given the limited data and the large number of parameters in the coupled model (38 for the plant model, 38+18 for the coupled model), we were facing an identifiability problem. Therefore, we had to drastically reduce the number of parameters that had to be estimated and proceeded as follows. We did an extensive literature review to inform parameter values and, when possible, directly computed parameters from experimental data, as described in Appendix C. In parallel we performed a global sensitivity analysis to determine the most influential parameters on the plant model variables, detailed in Section 3.2.1. Performing this analysis on the coupled model would have been too computationally costly; moreover, we had more information on root-knot nematode parameters, hence this choice. We thus narrowed down the estimation procedure to parameters that were influential or/and lacked robust estimates from the literature or experiments.

Parameter estimation was performed independently for both crop species. For each species, we proceeded in two steps. First, the parameters of the plant model were estimated using healthy (control) plant data. Second, these parameters were set in the plant–nematode model and the remaining nematode and interaction parameters were estimated using data from infected plants. At each step, the model was initialised using experimental data at time zero, given in Section 3.3. To compute the distance between data and model simulations, we used criteria based on the sum of normalised squared errors, given in Section 3.2.2. To minimise these criteria, we combined global and local optimisation algorithms described in Section 3.2.3. Finally, we assessed the robustness of our estimates using a bootstrap-inspired method defined in Section 3.2.4.

3.2.1 Global sensitivity analysis

We assessed the impact of parameter values on the plant model, the outputs of interest being plant model variables that vary over time. To account for the dynamical nature of our outputs, a multivariate global sensitivity analysis was conducted for each output, following the method by Lamboni et al. (2009, 2011).

1. First, the parameter space was explored using a fractional factorial design of resolution V, to estimate parameter main effects and two-way interactions. The design was obtained using the `planor` R package.

2. Second, a Principal Component Analysis (PCA) was applied, the individuals being the output simulated for all parameter combinations, and the variables being the output times. As a result, each simulation was given a "score" on each component. We then selected the first components explaining more than 95% of inertia.

3. Third, for each selected component, we used the Analysis of Variance to get the variance decomposition, based on a linear model with two-way interactions between the output score and the parameters. For each parameter main effect or interactions, we computed the Sobol sensitivity index (SI) as the ratio between the sum of squares of the term and the total sum of squares.

4. Fourth and finally, the generalised sensitivity index (GSI) of each term (main effect or interaction) was calculated as the sum of the sensitivity indices corresponding to the term on the selected PCA components, weighted by the inertia of the component.

This analysis was performed on eight outputs, corresponding to the plant state variables: the structural biomasses (W_s, W_r, W_f) and the carbon concentrations (C_s, C_r, C_f) in the three plant compartments, whose dynamics are described in (1), and the water potentials (ψ_s, ψ_r) in the shoots and roots, whose dynamics are given in (13). Among the plant parameters, some were set according to Section C.3. The 24 remaining parameters were varied over three levels, covering the range of reported literature values shown in Table 8. In total, 19683 simulations were performed.

3.2.2 Optimisation criteria

Based on the experimental data presented in Section 3.1, two criteria were used to calibrate the healthy plant model (1,13) and the coupled plant–nematode model (1,13,4,6). As the model was initialised using experimental data at time zero (inoculation time), only the two subsequent time points, at 6 and 12 weeks post-inoculation, were used for the parameter estimations.

For the healthy plant model The data available corresponding to plant model variables were the structural dry masses W_x of shoots ($x = s$), roots ($x = r$), and fruits ($x = f$). To make full use of the available measurements, we complemented these data with leaf count observations collected over the same experiment. To relate these observations to a model variable, an allometric relationship was established between the shoot dry mass (W_s) and the number of leaves (L_f), following the approach commonly used in the literature (Le Maitre and Midgley, 1991; Zeinali et al., 2014) and detailed in Section C.1.

The criterion to be minimised is hence the following sum of normalised squared errors:

$$\mathcal{E}_p = \pi_p^1 \underbrace{\frac{1}{2} \sum_{i=6,12} \left[\left(\frac{W_s^{\text{mod}} - W_s^{\text{obs}}}{W_s^{\text{std}}} \right)_{t=i}^2 + \left(\frac{W_r^{\text{mod}} - W_s^{\text{obs}}}{W_r^{\text{std}}} \right)_{t=i}^2 + \left(\frac{W_f^{\text{mod}} - W_s^{\text{obs}}}{W_f^{\text{std}}} \right)_{t=i}^2 \right]}_{\text{Control plant data}} + \pi_p^2 \underbrace{\frac{1}{12} \sum_{j=1}^{12} \left(\frac{W_s^{\text{mod}} - W_s^{\text{leaf}}}{W_s^{\text{leaf}}} \right)_{t=j}^2}_{\text{Additional leaf data}}. \tag{7}$$

Here, i indicates the two destructive data time points and j the 12 weekly non destructive data time points (time t in weeks); exponents "mod", "obs", and "std" correspond to model simulations, mean experimental observations (over six replicates), and their associated standard deviations, respectively; $\pi_p^1 = 0.8$ and $\pi_p^2 = 0.2$ are weighting coefficients. W_s^{leaf} represents the equivalent dry mass obtained from the allometric relation applied on the leaves measurements. This normalised criterion was chosen to give more weight to more consistent measures, the weighting coefficients to favour data directly linked to model variables.

For the coupled plant–nematode model As for the healthy plant model, the plant data available were the structural dry masses. To relate nematode data to model variables, the number of observed egg masses EM was equated to the number of mature females F, as a female produces a single egg mass. The mean number of eggs per egg mass EEM was compared to ρ/μ_F, where ρ is the nematode egg laying rate (5), which varies with carbon concentration and hence time, and $1/\mu_F$ represents the average time spent by a mature female in the egg-laying stage. The number of J_2 larvae in the soil was only measured at the end of the experiment ($t = 12$ weeks).

The number of galls observed G was approximated in the model as the number of mature females F plus a fraction ξ of larvae inside in the roots, a newly-formed gall being too small to be detected: $G \approx \xi J + F$. We estimated this fraction as $\xi = 1 - \tau\eta$, with $1/\eta$ the average duration of the within-root larval stage and τ the time required for the development of feeding sites, particularly the growth of giant cells, which become visible only several days after infection (Berg et al., 2009). Reported values of τ are approximately 7 days for tomato and 10 days for pepper, capturing the species-specific delay in gall appearance (Shepherd and Huck, 1989; Joshi et al., 2020). The number of galls was only measured at the first point ($t = 6$ weeks); at the second time point, galls are too numerous to count.

The criterion to be minimised is hence the following sum of normalised squared errors:

$$\mathcal{E}_c = \pi_c^1 \underbrace{\frac{1}{2}\sum_{i=6,12}\left[\left(\frac{W_s^{\mathrm{mod}}-W_s^{\mathrm{obs}}}{W_s^{\mathrm{std}}}\right)_{t=i}^2+\left(\frac{W_r^{\mathrm{mod}}-W_s^{\mathrm{obs}}}{W_r^{\mathrm{std}}}\right)_{t=i}^2+\left(\frac{W_f^{\mathrm{mod}}-W_s^{\mathrm{obs}}}{W_f^{\mathrm{std}}}\right)_{t=i}^2\right]}_{\text{Infected plant data}}$$
$$+\pi_c^2 \underbrace{\left[\frac{1}{2}\sum_{i=6,12}\left(\left(\frac{F^{\mathrm{mod}}-EM^{\mathrm{obs}}}{EM^{\mathrm{std}}}\right)_{t=i}^2+\left(\frac{\rho^{\mathrm{mod}}/\mu_F-EEM^{\mathrm{obs}}}{EEM^{\mathrm{std}}}\right)_{t=i}^2\right)\right.}_{\text{Nematode data}} \tag{8}$$
$$\underbrace{\left.+\left(\frac{J_2^{\mathrm{mod}}-J_2^{\mathrm{obs}}}{J_2^{\mathrm{std}}}\right)_{t=12}^2+\left(\frac{G^{\mathrm{sol}}-G^{\mathrm{obs}}}{G^{\mathrm{std}}}\right)_{t=6}^2\right]}_{\text{Nematode data}}.$$

As previously, i indicates the two destructive data time points (time t in weeks); exponents "mod", "obs" and "std" correspond to model simulations, mean experimental observations (over six replicates), and their associated standard deviations, respectively. Weighting coefficients $\pi_c^1 = 0.7$ and $\pi_c^2 = 0.3$ were chosen to give twice more weight to plant measures, which are easier to measure and hence more reliable.

3.2.3 Optimisation algorithm

In this study, we adopted a hybrid optimisation approach combining both global and local search algorithms to estimate the model parameters.

We first apply the *Adaptive Random Search* (ARS) algorithm, a stochastic global optimisation method that iteratively adjusts the search step (standard deviation) to efficiently explore the parameter space and approach the global optimum (Masri et al., 1980). The ARS requires two main inputs: the criterion to be minimised and the search domain defined by lower and upper bounds for each parameter. Because of its stochastic nature, several independent runs of the ARS were performed, each starting from a randomly selected point within the parameter bounds. The ARS algorithm was parametrised as follows. The number of iterations in the learning phase for each tested standard deviation was set to 200, while the number of iterations in the exploitation phase was set to 400. The maximum number of objective function evaluations was fixed at 10 000. The algorithm was deemed to have converged when the maximum number of successive uses of the smallest standard deviation, set to 2, was reached. These values were chosen to balance computational cost and robustness of convergence based on preliminary sensitivity analyses. The best solution among the runs that converged, i.e. the one yielding the lowest criterion value, was retained as the global optimum candidate.

Once the ARS provided a candidate solution, a local optimisation was carried out to refine the parameter estimates. For this purpose, we used the *Nelder–Mead simplex* method (Nelder and Mead, 1965), as implemented in the `scipy.optimize.minimize` function (Python, SciPy v1.11). The minimum requirement is the optimisation criterion. This two-step hybrid approach ensures both global exploration of the parameter space and precise local refinement of the final solution.

3.2.4 Bootstrapping

To evaluate parameter uncertainty and assess the robustness of parameter estimation, we employed a systematic, bootstrap-inspired approach. Bootstrapping is a resampling technique that estimates the variability of model parameters by repeatedly fitting the model to perturbed versions of the original dataset. Rather than relying on a single set of observations, this approach allows quantification of how sensitive parameter estimates are to the specific data points used for calibration.

Original parameter estimations were conducted for the two crop species and the two treatments, based on either healthy or infected plant data. Each of these four estimations was based on 18 independent plants, corresponding to six biological replicates destroyed and measured at three time points (0, 6 and 12 weeks post-inoculation).

For the bootstrap procedure, the resampling consisted in removing two biological replicates, which led to $\binom{18}{16} = 153$ combinations of 16 plants, constituting unique data subsets. Note that the removal of a biological replicate triggers the removal of all associated plant and nematode measures. Hence, 153 extra parameter estimations were conducted for each crop×treatment, i.e. in total $153 \times 2 \times 2 = 612$ estimations, based on the same optimisation criteria and algorithms as the original estimations. The resulting ensemble of parameter estimates provided an empirical distribution from which uncertainty bounds could be derived.

3.3 Initial conditions of the model

Unless specified otherwise, model initial conditions were set as follows. Most state variable initial values were derived from the data at time zero, provided in Table 6, namely:

- the plant dry masses
  - for tomato $W_s(0) = 0.25$ g, $W_r(0) = 0.06$ g, $W_f(0) = 0$ g;
  - for pepper $W_s(0) = 0.1$ g, $W_r(0) = 0.03$ g, $W_f(0) = 0$ g;
- the nematode populations $E(0) = 20000$ individuals, $J_2(0) = J(0) = F(0) = 0$;
- the gall mass $W_g(0) = 0$ g.

The initial carbon concentrations were set to arbitrary values: $C_s(0) = C_r(0) = 0.5$ and $C_f(0) = 0$.

The initial water potentials for shoots $\psi_s(0)$ and roots $\psi_r(0)$ were set according to (12), using the initial dry masses and replacing the leaf transpiration defined in (11) by $A = \sigma_W W_s(0)$ (no water stress initially, so $f_p(\psi_s) = 1$).

3.4 Definition of metrics

All indicators are based on a cropping season of $T = 100$ days, covering two nematode life cycles.

3.4.1 Plant carbon allocation

We defined three carbon-partitioning indicators describing how assimilated carbon is distributed among plant organs over a cropping season. All indicators represent the fraction of cumulative carbon allocated to a specific sink (roots or fruits) from a source (shoots). Let us define $U_c(t) =$

$k_s\, f_k(\psi_s)\, \frac{C_s}{K_s+C_s}\, W_s(t)$, the instantaneous carbon assimilation from shoots via the photosynthesis at time t.

- **Root allocation fraction** (RAF): this indicator measures the proportion of total assimilated carbon that is allocated to roots. It is defined as:

$$\mathrm{RAF} = \frac{\int_0^T T_r(t)\, dt}{\int_0^T U_c(t)\, dt},$$

  where $T_r(t)$ (16) is the carbon flux from shoots to roots at time t.

- **Fruit allocation fraction** (FAF): this indicator describes the proportion of assimilated carbon directed to fruits. It is defined as:

$$\mathrm{FAF} = \frac{\int_0^T T_f(t) + T_a(t)\, dt}{\int_0^T U_c(t)\, dt},$$

  where $T_f(t)$ (16) is the carbon flux from shoots to fruits and $T_a(t)$ (17) the active carbon transport toward fruits at time t.

- **Shoot maintenance fraction** (SMF): this indicator captures the remaining proportion of assimilated carbon that is retained by shoots for growth and maintenance. It is defined as:

$$\mathrm{SMF} = 1 - (\mathrm{RAF} + \mathrm{FAF}),$$

  ensuring that total carbon allocation fractions sum to unity.

3.4.2 Gall indicators

To quantify the impact of nematode infestation, we used several metrics of gall severity, which capture both the magnitude and temporal dynamics of gall development. We consider the total infesting nematodes (larvae $J(t)$ + mature females $F(t)$) as a proxy for the total number of galls at time t.

- **Mean gall weight** (MGW): it corresponds to the total gall biomass $W_g(t)$ per gall, averaged over the season. It is defined by:

$$\mathrm{MGW} = \frac{1}{T} \int_0^T \frac{W_g(t)}{J(t) + F(t)}\, dt,$$

- **Mean number of galls** (MNG): it corresponds to the total number of galls, averaged over the season. It is defined by:

$$\mathrm{MNG} = \frac{1}{T} \int_0^T J(t) + F(t)\, dt.$$

- **Mean gall proportion of the total root system** (MGP): this indicator reflects the average fraction of total root mass composed of galls, highlighting the systemic burden imposed on the root system over time. It is defined by:

$$\mathrm{MGP} = \frac{1}{T} \int_0^T \frac{W_g(t)}{W_g(t) + W_r(t)}\, dt.$$

- **Gall index proxy** (GIP): it measures the end-of-season proportion of root biomass composed of galls, offering a snapshot of the cumulative impact of infestation on the final root structure. It is defined by:

$$\text{GIP} = \frac{W_g(T)}{W_g(T) + W_r(T)}.$$

3.4.3 Tolerance indicator

Plant tolerance was quantified by the **tolerance index** (θ), which measures the plant ability to maintain its yield under nematode infestation. Based on a commonly used proxy of plant yield (Nilusmas et al., 2020), namely the integral of the healthy shoot dry mass during a cropping season T:

$$\widehat{W_s} = \int_0^T W_s(t)\, dt,$$

the tolerance index θ is expressed as follows:

$$\theta = \frac{\widehat{W_s^{\mathrm{i}}}}{\widehat{W_s^{\mathrm{h}}}}, \tag{9}$$

where W_s^i and W_s^h are the yield proxies in the presence and absence of nematodes, respectively. So, $\theta = 0$ refers to a very susceptible plant, while $\theta = 1$ corresponds to a highly tolerant plant. We further consider $\theta = 0.65$ as a tolerance threshold, assuming that a plant must maintain at least 65% of its potential yield despite parasitism in order to be considered tolerant.

Note that, for the sensitivity analyses performed on the tolerance index, the model output is scalar rather vectorial. As a result, the procedure described in Section 3.2.1 is simplified in this case: no principal component analysis is required.

3.4.4 Epidemiological indicator

We defined the **seasonal nematode reproduction factor** (ζ) to describe the magnitude of nematode population increase or decrease at the end of a cropping season T. It is computed as the ratio between the final and initial numbers of free-living nematodes:

$$\zeta = \frac{E(T) + J_2(T)}{E(0)}. \tag{10}$$

Both eggs (E) and juvenile larvae (J_2) are included at time T, but only eggs at time 0, according to the initial conditions defined in Section 3.3.

Note that for a plant to be tolerant, it should not only preserve its yield under nematode infestation, but it should also allow nematode development, which could be assessed by the seasonal nematode reproduction factor. Otherwise, it would be considered as a resistant plant. However in this study, the plants we considered were not resistant, so we did not use this factor to assess their tolerance.

4 Results

We first concentrate on the results of the calibration procedure, which show that the model can describe the dynamics of tomato and pepper, with or without RKN induced-biotic stress. The

two crop species were selected for their contrasted responses to RKN infestation observed in the field. In Section 4.2, mostly based on the comparison of both crop species but not only, we investigate the traits underlying plant tolerance.

4.1 Calibration to experimental data

During the calibration procedure, to avoid identifiability issues, we set some parameter values based on the literature or directly computed them from the experimental data, as described in Appendix C. Model fits are displayed in Section 4.1.1 and parameter estimates in Section 4.1.2.

4.1.1 Model fits for the two crop species

Healthy plants The sensitivity analysis in Section C.4 identified four influential parameters. In addition, two parameters were included in the estimation process: the active transport rate to fruits (t_a), which is difficult to quantify experimentally, and the phloem resistance coefficient (r_{ph}), which influences carbon allocation patterns. Altogether, six parameters were therefore estimated for both tomato and pepper. The remaining parameters were set from experimental data or the literature, as detailed in Section C.5.1. The estimation results, including the parameter admissible ranges, are provided in Table 1, together with the fixed parameters. The model fits are illustrated in Figure 3.

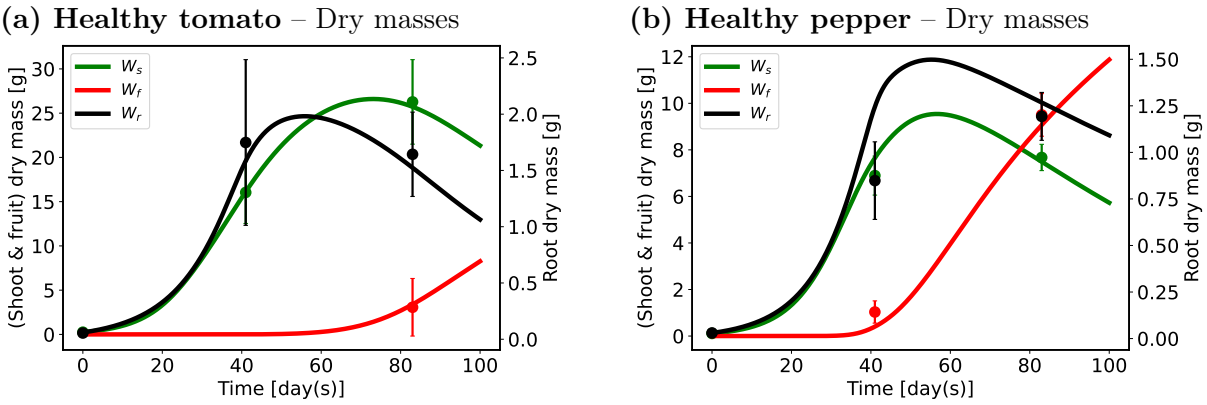

Figure 3: Calibration of the healthy plant model (1,13) on tomato and pepper control data. Dry mass simulations (curves) and data points (mean and standard deviations) for shoots ($W_s(t)$, green), roots ($W_r(t)$, black), and fruits ($W_f(t)$, red). Data are listed in Table 6, model parameter values in Table 1, and initial conditions in Section 3.3.

This figure shows a good fit for both crop species. The model captures the slowdown of the vegetative growth once fruits emerge, illustrating the competitive carbon allocation between organs. This transition occurs earlier in pepper, which is consistent with the higher estimated active transport rate t_a (see Table 1).

More illustrations of the healthy plant dynamics for both species are provided in Section D.1.

Infested plants Contrary to the healthy plant calibration, the selection of nematode and interaction parameters to be estimated was not based on a sensitivity analysis. Whenever possible, parameters were set to experimentally-derived or literature-based values, as detailed in Section C.5.2. Only five parameters for which reliable information was lacking were estimated in both species: the nematode infection rate (β), the feeding rate (γ), the gall growth rate (k_g), the

half-saturation constant for reproduction (K_ρ), and half-saturation constant for establishment efficiency coefficient (K_ω). The estimation results, including the parameter admissible ranges, are provided in Table 2, together with the fixed parameters. The model fits are illustrated in Figure 4 and Figure 5.

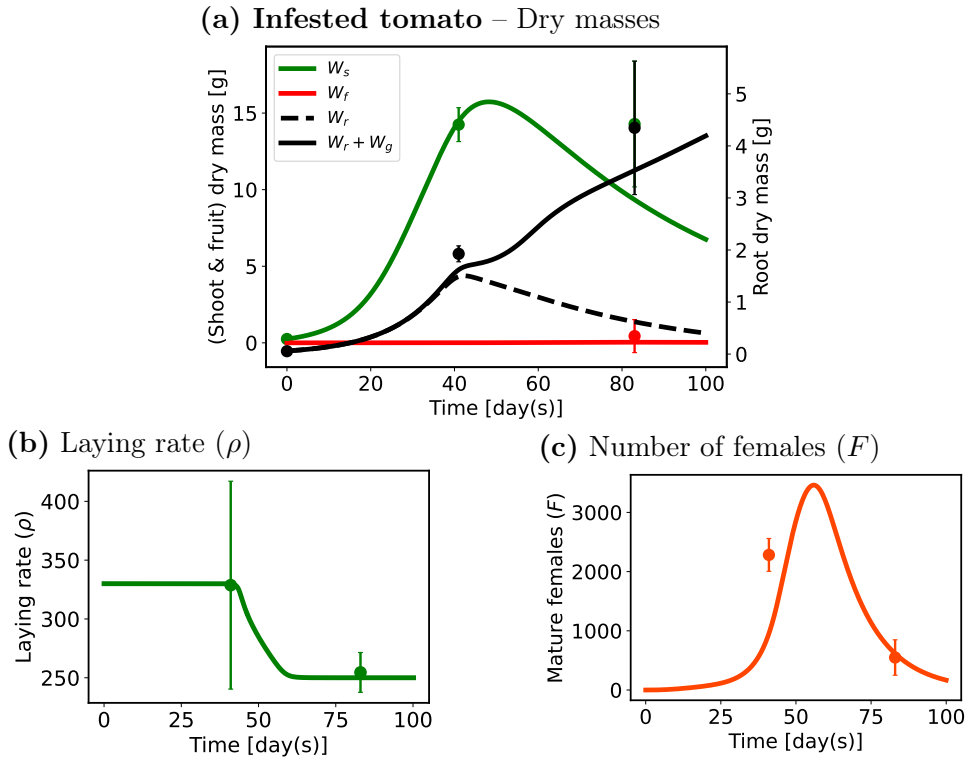

Figure 4: Calibration of the coupled plant–RKN model (1,13,4,6) on infested tomato data. (a) Dry mass simulations (curves) and data points (mean and standard deviations) for shoots ($W_s(t)$, green), total roots ($W_r(t)+W_g(t)$, black), healthy roots ($W_r(t)$, dashed black), and fruits ($W_f(t)$, red). (b) Laying rate ($\rho(C_r(t))$), simulated from model equation (5). (c) Mature females ($F(t)$). Data are listed in Table 6 and Table 7, model parameter values in Table 1 and Table 2, initial conditions in Section 3.3.

For both crop species, simulations of the coupled model match the experimental data well. Compared to the healthy plant, shoot and fruit growth under nematode infestation is markedly reduced for tomato, but only slightly so for pepper. Fruit growth is almost completely suppressed for tomato, while it remains comparable to the healthy case for pepper. Nematodes act as an additional carbon sink with a strong sink strength: they divert assimilated carbon towards the root system to sustain their own development. As a consequence, the total root mass is higher compared to the healthy plant, but because of galls, especially for tomato. Furthermore, nematodes enter the roots more rapidly and are more abundant at their peak in tomato than in pepper. These results are consistent with pepper being more tolerant than tomato to RKN infestation.

More illustrations of the infested plant dynamics for both species are provided in Section D.2.

4.1.2 Comparison of plant parameter estimates

We compared the estimated parameters for tomato and pepper to identify potential physiological traits associated with tolerance.

Several plant parameters differ between the two species (Figure 6(a)). Pepper exhibits a

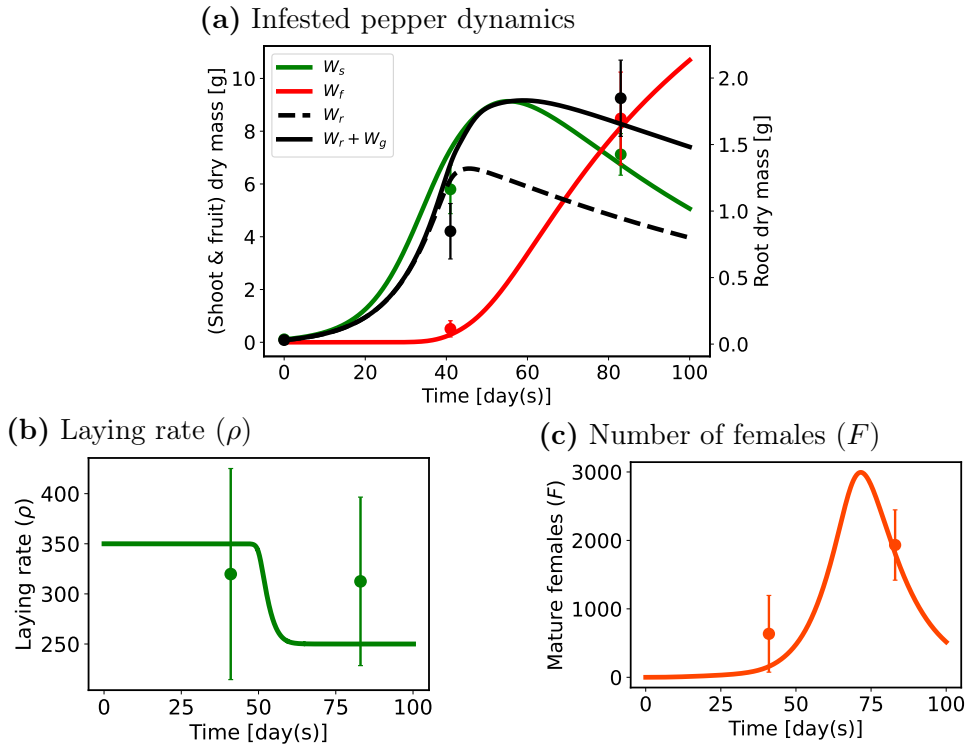

Figure 5: Calibration of the coupled plant–RKN model (1,13,4,6) on infested pepper data.(a) Dry mass simulations (curves) and data points (mean and standard deviations) for shoots ($W_s(t)$, green), total roots ($W_r(t)+W_g(t)$, black), healthy roots ($W_r(t)$, dashed black), and fruits ($W_f(t)$, red). (b) Laying rate ($\rho(C_r(t))$), simulated from model equation (5). (c) Mature females ($F(t)$). Data are listed in Table 6 and Table 7, model parameter values in Table 1 and Table 2, initial conditions in Section 3.3.

slightly higher photosynthesis rate (p), a higher active transport rate (t_a), and a lower root mortality rate (d_r), suggesting stronger carbon assimilation and greater sink strength of fruits in pepper. Tomato, in contrast, shows a higher fruit growth rate (k_f) and a higher phloem resistance coefficient (r_{ph}), highlighting its greater accumulation of fruit biomass but potentially reduced phloem transport efficiency. These differences collectively point to distinct carbon allocation strategies and fruit developement between species.

For nematode-related parameters (Figure 9(b)), tomato displays higher infection rate (β), feeding rate (γ), half-saturation constants for reproduction (K_ρ) and establishment (K_ω), and gall-xylem resistance coefficient (ϕ). These elevated parameters indicate that nematodes infect, feed, and develop more effectively on tomato roots, and that galls exert stronger a resistance on xylem flow.

(a) Physiological plant parameters

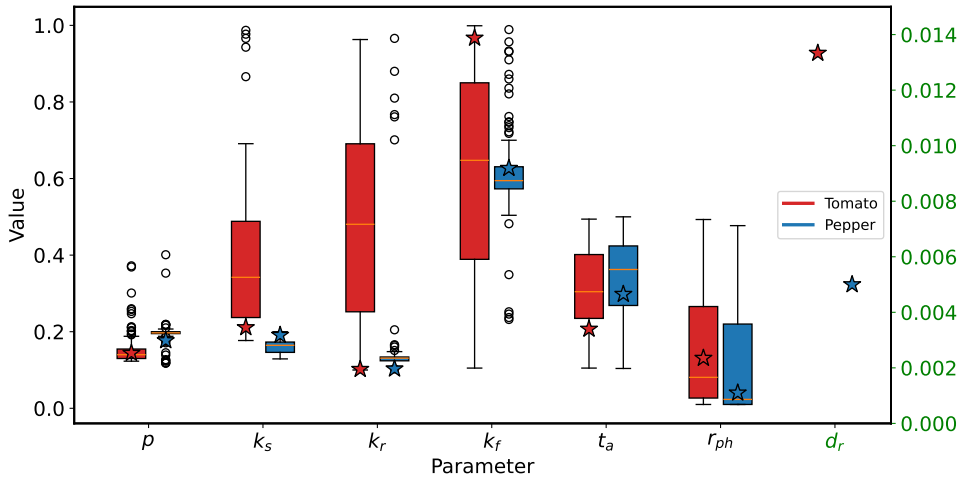

(b) Nematode-related interaction parameters

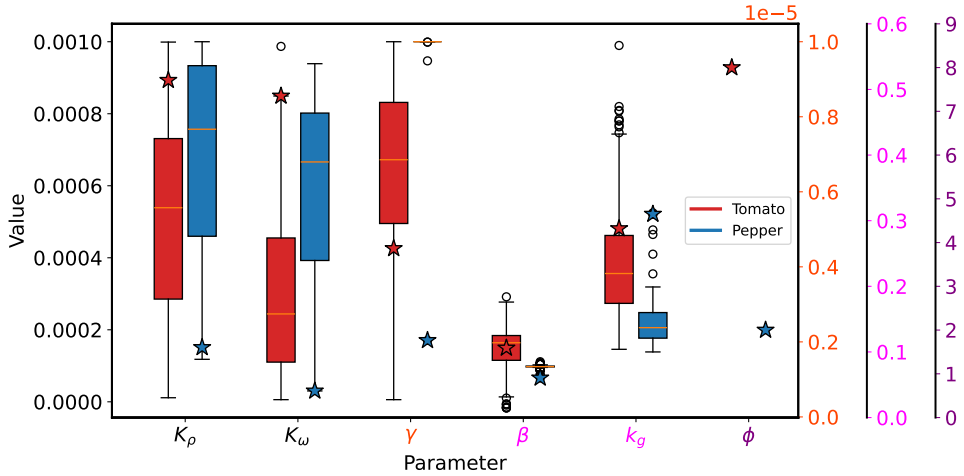

Figure 6: Comparison of estimated parameters for tomato (red) and pepper (blue). Panels show (a) physiological plant parameters and (b) nematode-related interaction parameters. Stars denote parameter estimates obtained from the full dataset prior to bootstrapping, while the boxplots depict the bootstrap-derived uncertainty around those estimates. Parameters without boxplots were not estimated but differ between species.

4.2 Identifying plant tolerance mechanisms

Parameter comparisons in Section 4.1.2 pointed out differences in carbon allocation towards plant compartments and galls, which are further quantified in Section 4.2.1. We then used the tolerant pepper traits to virtually improve tomato tolerance in Section 4.2.2 and assessed the robustness of these traits under different RKN-virulence scenarios in Section 4.2.3. Finally, we broadened our search for tolerance traits beyond the pepper-based traits in Section 4.2.4.

4.2.1 Contrasted carbon allocations

Carbon allocation differed markedly between tomato and pepper, and these differences were amplified under nematode infestation, as shown in Figure 7. When combined with the gall metrics in Figure 8, they provide a mechanistic understanding of the different plant responses to RKN infestation.

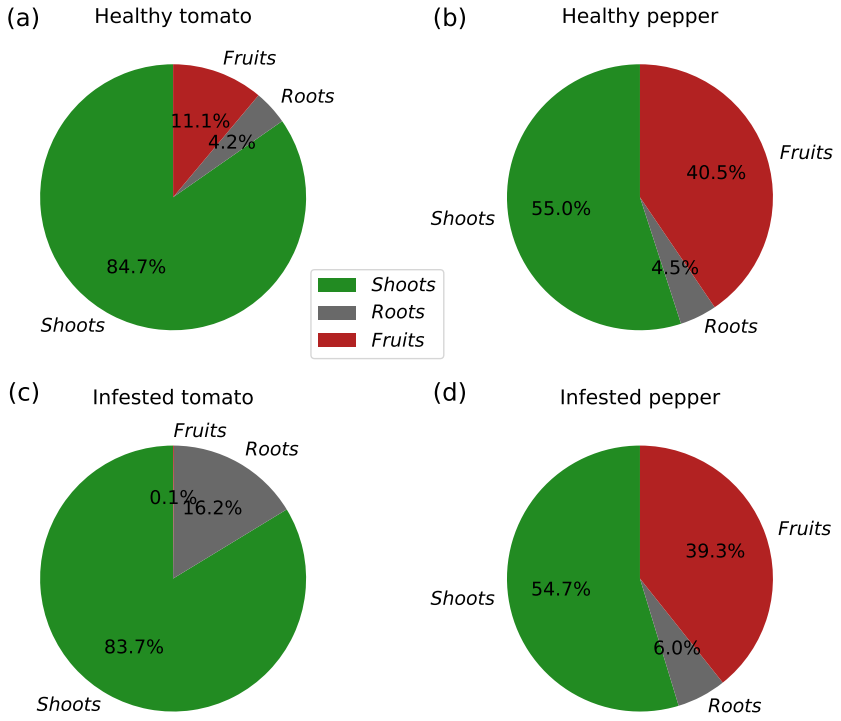

Figure 7: Carbon allocation in healthy and infested tomato and pepper, based on indicators defined in Section 3.4.1: percentage of carbon allocated to shoots (SMA, blue), roots (RAF, orange), and fruits (FAF, green).

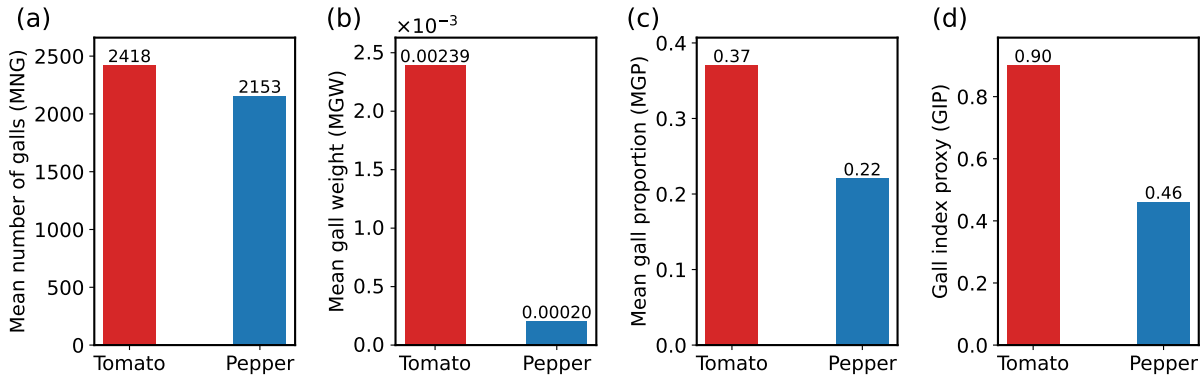

Figure 8: Gall metrics for tomato (red) and pepper (blue), based on the indicators described in Section 3.4.2.

Healthy tomato and pepper exhibit intrinsically different allocation strategies In healthy tomato, 11.1% of the carbon stored in shoots is allocated to fruits and 4.2% to roots (Figure 7(a)). Healthy pepper, in contrast, directs 40.5% to fruits and 4.5% to roots (Figure 7(b)), demonstrating a much stronger reproductive pull. These baseline differences reflect contrasting growth strategies: tomato maintains a predominantly vegetative allocation profile, whereas pepper establishes an early and substantial fruit sink, as evidenced by its higher active fruit transport rate t_a (see Table 1). This inherent divergence sets the stage for understanding how nematode infestation alters carbon reallocation.

Galls strongly redirect carbon toward the roots in tomato In infested tomato, allocation to fruits collapses, whereas allocation to roots increases sharply (Figure 7(c)). This rise does not reflect enhanced root growth but rather the need to sustain RKN proliferation through gall formation, as evidenced by the decline in healthy root biomass shown in Figure 4(a). Gall metrics in Figure 8(b,c) reinforce this interpretation: the proportion of root mass composed of galls is markedly higher in tomato than in pepper.

The gall index proxy is consistent with the observations of Jauzion-Graverolle et al. (2025). At the end of the experiment, the number of galls was approximated by gall severity indices (Zeck, 1971): 6 was reported for tomato, corresponding to a major functional impairment of the root system, with up to 50% of the roots rendered non-functional because of galls; 3 was reported for pepper, corresponding numerous small galls, some of which have merged, but without yet compromising root function. Our results reflect the same pattern, the gall index proxy in tomato is approximately twice that observed in pepper (Figure 8(d)).

Pepper maintains a more balanced allocation pattern under infestation In infected pepper, allocation to roots increases moderately, while allocation to fruits remains high (Figure 7(d)). This indicates that pepper sustains a strong competing sink for fruits that prevent galls from monopolizing carbon resources. Gall metric in Figure 8(a) indicates that galls are not negligible in pepper roots in terms of quantity, but they are much smaller and lighter than for tomato, as shown in Figure 8(b,c).

These results suggest that a strong carbon allocation towards fruits and small galls may protect the plant from RKN-induced damages.

4.2.2 Towards a virtual tolerant tomato: pepper-inspired traits

From Figure 6(a), we identified five plant parameters that exhibited substantial interspecific differences: fruit growth rate (k_f), active transport rate (t_a), phloem resistance coefficient (r_{ph}), photosynthesis rate (p), and root mortality rate (d_r). To assess whether these traits are determinants for tolerance, we simulated virtual tomato plants by simultaneously varying these parameters within ranges used for the estimation and sensitivity analysis. All other plant and nematode parameters were kept fixed at their values in Table 1 and Table 2.

To explore the parameter space, we used a full factorial design. For each plant trait, in addition to the estimated values for tomato and pepper, two intermediate uniformly-spaced values were included, as well as one similarly-spaced value outside the tomato-pepper interval. This resulted in a total of five levels per parameter. The full factorial design yielded to $5^5 = 3125$ parameter combinations.

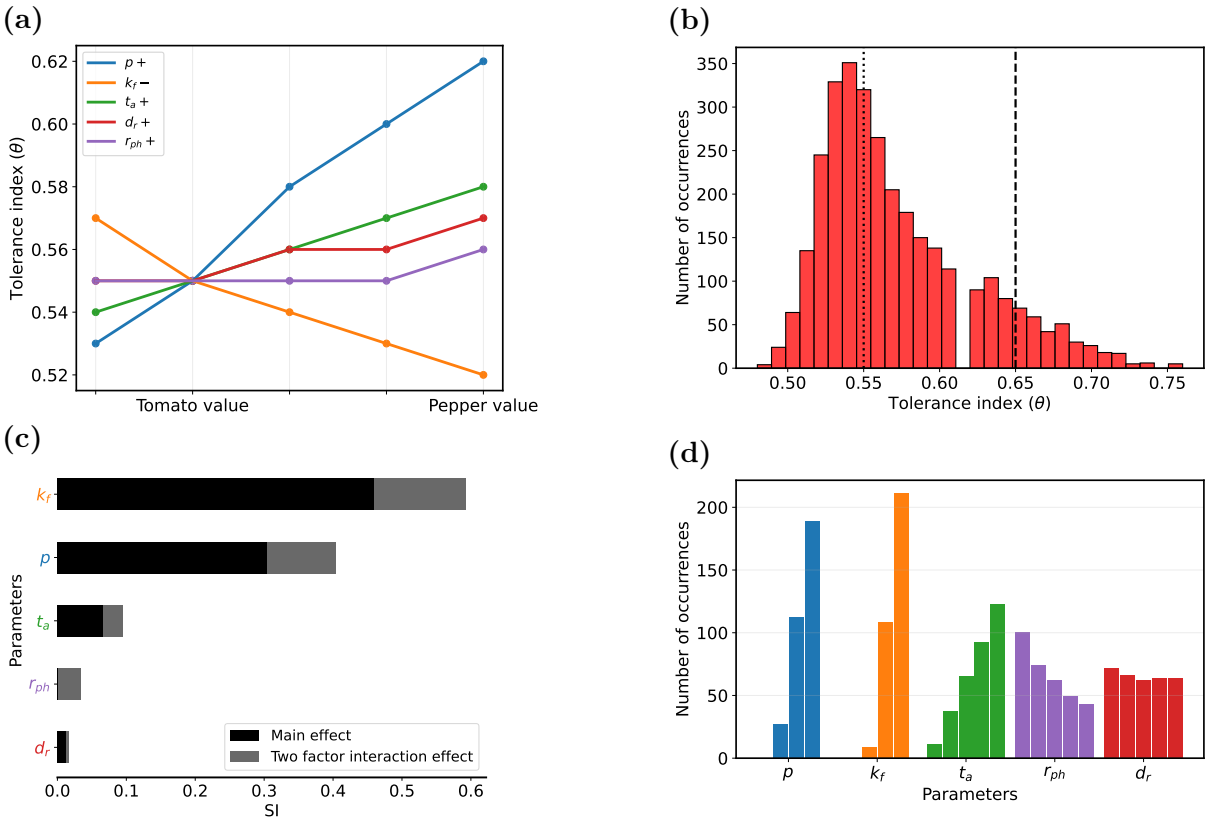

Figure 9: Evolution of the tolerance index (θ) by: (a) varying one parameter at a time while keeping all others fixed at their default values (Table 1, Table 2); Increasing (solid lines: tomato < pepper) or Decreasing (dashed lines: tomato > pepper); (b) varying all parameter combinations simultaneously; the dotted vertical line corresponds to the tolerance index of real tomato ($\theta = 0.55$), while the dashed line represents the tolerance threshold ($\theta = 0.65$); (c) sensitivity analysis of θ applied to the 3125 parameter combinations and (d) histogram of parameters for which $\theta \geq 0.65$.

The results show that the tolerance index increased substantially when the selected traits were shifted toward pepper values, with the exception of the fruit growth rate (k_f), which is higher in tomato (Figure 9(a)). Several virtual scenarios even outperformed the tolerance threshold (dashed vertical line, $\theta = 0.65$), suggesting that combining pepper-inspired traits has strong potential to enhance tolerance (Figure 9(b)). In particular, high values of the photosynthesis

rate (p), fruit growth rate (k_f), and, to a lesser extent, the active transport rate (t_a) strongly promote tolerance (Figure 9(d)). The wide distribution of tolerance indices could indicate that tolerance may emerge from both individual traits and their interactions. However, Figure 9(c) shows that interactions among traits play a relatively minor role compared to the contributions of individual traits.

4.2.3 Robustness of tolerance traits

The goal of this section is to assess whether the tolerance-related traits identified in Section 4.2 remain effective under varying levels of nematode pressure.

To this end, we defined three epidemic scenarios by varying two key epidemiological parameters: the infection rate (β), which governs the ability of nematodes to invade plant roots, and the maximum egg-laying rate ($\rho_{\max}$), which sets the upper limit of egg production per female under optimal conditions (Table 3). For each scenario, we evaluated the tolerance index (θ) (9) and the seasonal nematode reproduction factor (ζ) (10). These indicators were computed for the real tomato (Case 0) and for virtual tomato plants (Cases 1–5) in which one tolerance trait at a time was replaced by its pepper counterpart (Table 4). Figure 10(a) shows that the tolerance index was only slightly affected by the epidemic scenarios. It tended to decrease when the virulence increased, but the ranking among cases was maintained. In contrast, the reproduction factor increased markedly with virulence (Figure 10(b)), revealing important trade-offs among trait combinations. Notably, Case 1 (high photosynthesis rate p) and Case 3 (low phloem resistance r_{ph}) reached relatively high tolerance levels but also strongly amplified nematode populations.

Table 3: Definition of epidemic scenarios based on different levels of RKN virulence, determined by two key parameters: the infection rate (β) and the maximum rate of egg-laying ($\rho_{\max}$). Other parameters are fixed to their default values in Table 2.

Virulence	Infection rate (β)	Maximum egg-laying rate ($\rho_{\max}$)
Low	-30%	-30%
Medium	–	–
High	$+30\%$	$+30\%$

Note: Default tomato parameter values (–) or default values $\pm 30\%$ were used (see Table 2).

Table 4: Definition of the virtual tomatoes. Case 0 corresponds to tomato with its default parameter values (Table 1), while in Cases 1–5 one parameter at a time is replaced by its pepper value (as the points furthest to the right of Figure 9(a)). All remaining parameters were kept at the baseline tomato values specified in Table 1.

Tomato	Tolerance traits			
	p	t_a	r_{ph}	d_r
Case 0 (real)	to	to	to	to
Case 1 (virtual)	**pe**	to	to	to
Case 2 (virtual)	to	**pe**	to	to
Case 3 (virtual)	to	to	**pe**	to
Case 4 (virtual)	to	to	to	**pe**
Case 5 (virtual)	**pe**	**pe**	to	to

Note: to = tomato value; pe = pepper value.

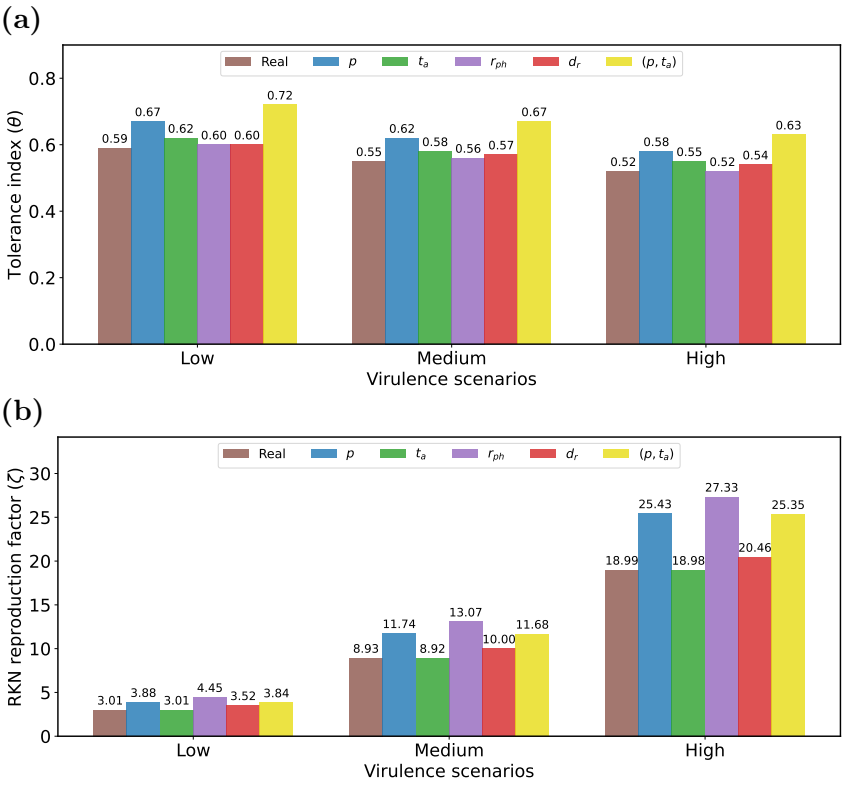

Figure 10: Robustness of tomato tolerance traits under different epidemic scenarios defined in Table 3. (a) Tolerance index (θ) and (b) nematode reproduction factor (ζ) for real (Case 0) and virtual (Cases 1–5) tomatoes defined in Table 4.

By contrast, Case 2 (high active transport rate t_a) offered a more desirable compromise: it produced one of the highest tolerance values while keeping the reproduction factor comparatively low.

4.2.4 Are there other tolerance traits?

Beyond the tolerance-related traits identified in Figure 6(a) and Figure 9, we aimed to investigate whether additional mechanisms could underlie plant tolerance. To this end, we considered a broader set of plant parameters that, according to the literature, may influence tolerance (Trudgill and Cotes, 1983; Wallace, 1987; Wise and Abrahamson, 2005; Ney et al., 2013). These additional traits were the growth rates (k_s, k_r) and mortality rates (d_s, d_r) of shoots and roots, xylem resistance (r_{xy}), transpiration rate (σ_W) and the allometry coefficient (α).

A sensitivity analysis on the tolerance index (θ) was then performed to evaluate the relative influence of these 11 parameters. Each parameter was varied across three levels spanning the range of trait values documented in the literature (Table 8). Simulations were performed using a fractional factorial design of resolution V, to estimate parameter main effects and two-way interactions. In total, 729 simulations were carried out.

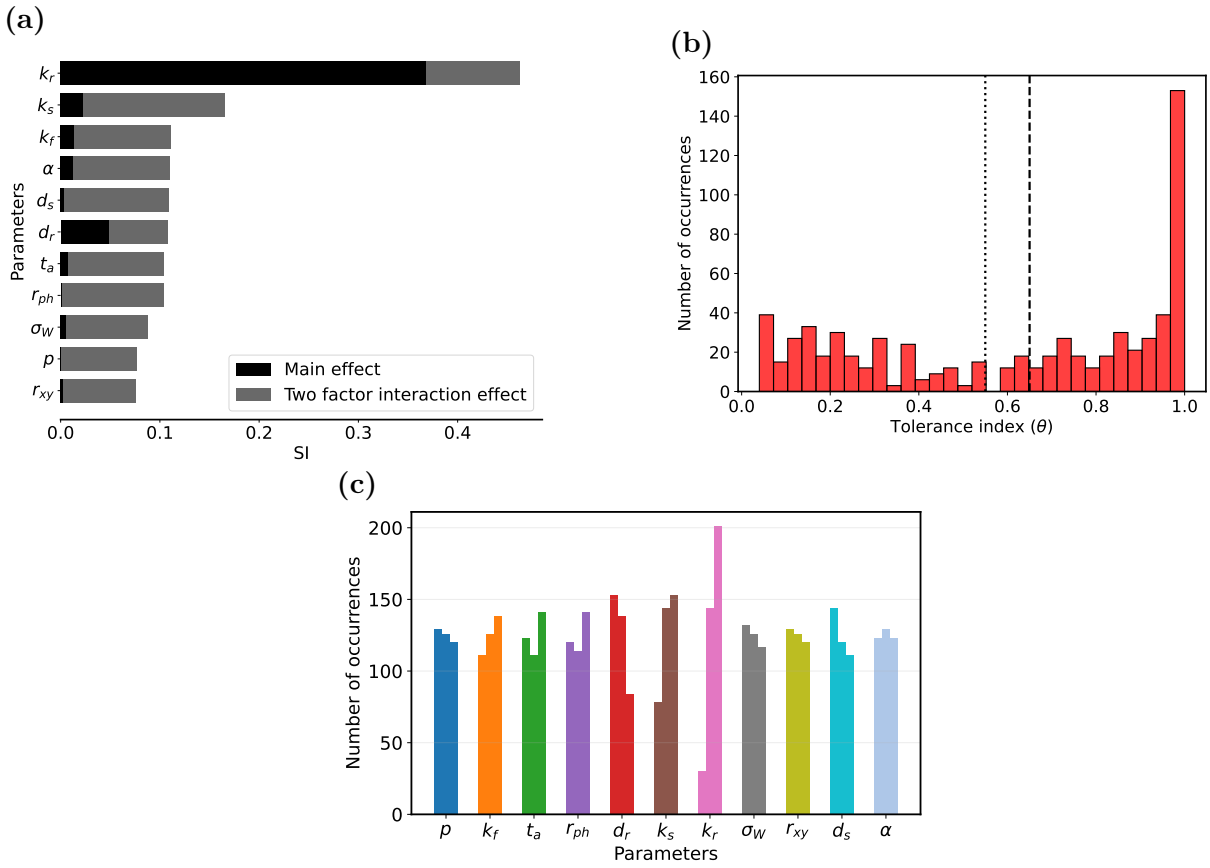

Figure 11: (a) Global sensitivity analysis on the tolerance index (θ); (b) histogram of the tolerance index (θ) for all 729 parameter combinations; the dotted vertical line corresponds to the tolerance index of real tomato ($\theta = 0.55$), while the dashed line represents the tolerance threshold ($\theta = 0.65$); (c) histogram of parameters for which $\theta \geq 0.65$.

Figure 11(a) shows two additional plant traits with high Sobol indices (SI ≥ 0.1) that strongly influence tolerance to RKN infection: the growth rates of roots (k_r) and shoots (k_s), both of which tend to act as compensatory mechanisms during nematode attack. A higher k_r favours a rapid growth of the root system, thereby diluting RKN infestation and maintaining a larger pool of functional roots. This vigorous root growth also stabilizes water uptake, which supports shoot growth and yield. A higher k_s helps maintain photosynthetic capacity through sustained biomass accumulation, ensuring sufficient carbon supply for tissue maintenance and repair, and ultimately supporting yield under infestation.

It should be noted that, except for the growth rate of roots (k_r), interactions dominate, so there may be synergistic or antagonistic trait combinations to generate tolerance (Figure 11(a,b)). In particular, moderate carbon acquisition capacity p, vigorous vegetative growth (shoots k_s and roots k_r), and high carbon allocation towards fruits (t_a, k_f), while, to a lesser extent, low shoot transpiration (σ_W) and xylem hydraulic resistance (r_{xy}) contribute to improving plant tolerance, as shown in Figure 11 (c).

5 Discussion

This study demonstrates that explicitly coupling plant physiology with root-knot nematode (RKN) demography provides a deeper insight into the mechanisms by which host condition both constrains and is constrained by RKN development. The modelling approach combines

several strengths rarely found together in plant–pest models: (i) inclusion of the plant reproductive phase through a distinct fruit compartment; (ii) explicit representation of water and carbon resources; (iii) coupling of plant physiological functions to nematode developmental stages; and (iv) incorporation of the role of plant carbon in infection dynamics. This coupling reveals that root carbon availability acts as a central integrator of plant condition, regulating both the establishment success and reproductive output of nematodes (Moens et al., 2009).

The coupled model was calibrated using two horticultural crop species with contrasting physiological traits: tomato and pepper. Model fits closely matched these contrasted dynamics. In the healthy state, calibrated parameters reproduced species-specific growth trajectories, particularly the earlier and stronger fruit sink in pepper. Under infestation, simulations accurately captured the suppression of tomato fruit growth, the diversion of carbon to gall biomass, and the milder shifts observed in pepper. The model also reproduced nematode traits such as laying rate, female abundance, and gall development, confirming that the calibrated parameters effectively reproduces the species-specific infection outcomes. Contrasting parameters and traits between tomato and pepper explain their divergent physiological behaviour to RKN infestation. In tomato, infestation produces a strong redirection of assimilates toward the root system, driven by the high sink strength of galls. This causes a collapse of fruit allocation and a major reduction in vegetative growth, consistent with the high gall biomass, large gall index, and early depletion of healthy roots observed experimentally. In pepper, by contrast, the strong intrinsic fruit sink limits the dominance of galls, allowing the plant to maintain both reproductive growth and moderate root allocation despite infection.

However, although our model can reproduce general field observations, some caution is warranted. For instance, the experiments of Jauzion-Graverolle et al. (2025) over which our model is calibrated, were conducted in pots, a condition known to restrict root expansion, alter root architecture, and increase local gall density by limiting available soil volume. Such spatial constraints can exaggerate gall severity, particularly in species with vigorous root systems such as tomato. Thus, while the magnitude of gall indices is informative, their interpretation must account for experimental context. Furthermore, nematode densities at the end of the season may be higher than predicted due to factors not captured by the model, such as migration to neighboring plants, survival on alternative hosts, or delayed hatching of dormant eggs (Moens et al., 2009; Sikora et al., 2018). This limitation, linked to the use of isolated potted plants, exists throughout the season but may have a greater impact at the end of the cycle, particularly if the plant is weakened, which increases the likelihood of nematode migration. It may also be relevant at the beginning of the season, for example in cases of high initial infestation, which we did not explore. Accounting for these processes could improve predictions of nematode population build-up and refine the assessment of long-term epidemiological risk.

Our results showed that tolerance does not depend on a single factor but can arise through multiple physiological pathways. Virtual experiments showed that a single trait can be sufficient to generate tolerance, but specific trait combinations may quantitatively improve yield maintenance under RKN infection. In particular, high photosynthetic capacity, vigorous vegetative and root growth, and a robust carbon allocation toward fruits all contribute positively to tolerance. These traits provide complementary advantages: increased root growth dilutes the local impact of gall formation while sustaining water and nutrient uptake; a strong fruit sink, particularly early in the infection process, helps draw carbon away from parasitised roots and prevents ex-

cessive depletion of vegetative organs; enhanced photosynthetic capacity supports overall plant functioning as well as the additional metabolic demands imposed by the parasite. In addition, the tolerant traits identified by the model are consistent with conceptual frameworks of plant tolerance to biotic stress, in which compensatory growth and sustained resource acquisition mitigate pathogen impact without reducing pathogen multiplication (Wise and Abrahamson, 2005; Ney et al., 2013). These traits therefore emerge as strong candidate targets for breeding strategies aimed at improving tolerance to root-knot nematodes.

Among the multiple traits contributing to tolerance, fruit dynamics emerge as a particularly influential factor. Early and strong fruit sinks, as observed in pepper, compete effectively with galls for carbon and limit excessive allocation to infected roots, thereby reducing nematode-driven resource hijacking. However, fruit dynamics in tomato was constrained by the limited data available and by an experimental period that was likely too short relative to the onset of flowering. Consequently, parameter estimates for tomato fruit traits such as fruit growth rate (k_f) and active transport (t_a) should be interpreted with caution. Overall, these findings highlight reproductive phenology, rarely considered in plant–pest models, as a major axis of tolerance. The latter suggests that plants with early reproductive traits could be advantageous in managing RKN parasitism.

Although tolerance preserves yield, it may inadvertently sustain or enhance nematode population build-up, with epidemiological consequences at the cropping-system scale. Consistent with theory (Trudgill and Cotes, 1983; Bishop, 2012), our simulations show that pepper-like trait sets maintain high productivity under infestation while consistently allowing moderate to high nematode reproduction. This result reinforces the classical notion that tolerance, unlike resistance, does not limit nematode multiplication. Consequently, tolerant cultivars may be agronomically advantageous within a single season but could contribute to long-term soil contamination, particularly in crop rotations that include susceptible species. Evaluation of tolerant cultivars should therefore integrate both agronomic and epidemiological criteria. In practice, this implies careful management of rotations and the possible use of soil sanitation or other mitigation techniques during intercultural periods to limit nematode carry-over.

The coupled plant–RKN model developed in this work demonstrated substantial versatility, as evidenced by its ability to reproduce plant–nematode interactions across contrasting species, biotic pressures, and abiotic conditions within a single structural formulation. In our study, the same set of model equations successfully captured growth, carbon allocation, and infection dynamics in both tomato and pepper, requiring only species-specific parameterisation. Beyond interspecific differences, the model responded realistically to a broad gradient of infestation pressures, from low inoculum densities to severe attacks, reproducing expected shifts in plant carbon limitation, gall expansion, and nematode reproduction (Section 3.4.1). Importantly, the framework proved equally robust under abiotic stress scenarios, including shading and water stress. In both cases, it correctly predicted well-established physiological responses: enhanced shoot growth at the expense of roots under shading, and the opposite pattern under water stress, as shown in Section D.3. The ability of a single set of core equations to accommodate interspecific variation as well as biotic and abiotic perturbations indicates that the proposed model is not restricted to a narrow ecological context.

Therefore, the framework opens several avenues for future research. Coupling the model with soil nematode dynamics over multiple cropping seasons would enable evaluation of the long-term

impacts of tolerance on field epidemiology (Nilusmas et al., 2020; Tankam-Chedjou et al., 2020). Incorporating environmental drivers, such as temperature variation or soil moisture, could reveal interactions between abiotic and biotic stress tolerance. Moreover, genetic variability could be accounted for by linking model parameters to measured traits across multiple cultivars.

Thanks to its versatility, this modeling framework could readily be extended beyond RKN to other biotic or abiotic stresses and to additional horticultural crops, thereby contributing to the design of resilient cropping systems. This approach thus underscores the value of mechanistic, host-centered perspectives in studying plant–pest interactions.

A Model complements

A.1 Water transport modelling

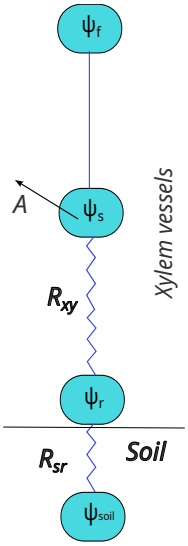

Figure A.12: Diagram of water transport in the plant. Water potentials (ψ) decrease from soil to roots (index r), and roots to shoots/fruits (indices s/f), depending on hydraulic resistances (R). The water flow (A) is assumed to be "at equilibrium" in the plant.

Water transport is illustrated in Figure A.12. We assume that the water potential of the soil ψ_{soil} is constant and that the water potentials of the shoots and fruits are equal, that is $\psi_s = \psi_f$.

Leaf transpiration drives the water transport and is defined as follows :

$$A = \sigma_W \, W_s \, f_p(\psi_s). \tag{11}$$

It is proportional to the shoot biomass and it decreases in case of water stress.

The water fluxes, expressed through the water potentials from soil to roots (ψ_r) and from roots to shoots (ψ_s), are described as follows:

$$\psi_r = \psi_{\text{soil}} - R_{sr} A \quad \text{and} \quad \psi_s = \psi_r - R_{xy} A = \psi_{\text{soil}} - (R_{sr} + R_{xy}) A, \tag{12}$$

where the hydraulic resistance between soil and roots is:

$$R_{sr} = \frac{r_{sr}}{W_r^{\alpha_r}},$$

and the xylem resistance between roots and shoots is:

$$R_{xy} = R_{xy,s} + R_{xy,r}, \quad \text{with: } R_{xy,s} = \frac{r_{xy,s}}{W_s^{\alpha_s}} \text{ and } R_{xy,r} = \frac{r_{xy,r}}{W_r^{\alpha_r}}\left(1 + \phi\frac{W_g}{W_g + W_r}\right).$$

We assume that galls do not contribute to water transport, which is why the healthy root biomass and not the total root biomass is in the denominator of the xylem resistance in the roots $R_{xy,r}$. Moreover, the presence of galls hinders water transport in the roots, so we assume that $R_{xy,r}$ increases with gall biomass by a factor of at most $1 + \phi$.

We then derive equations (12) and obtain the dynamics of the water potentials:

$$\begin{aligned}
\frac{d\psi_s}{dt} &= -\left[A\left(\frac{dR_{sr}}{dt} + \frac{dR_{xy}}{dt}\right) + \sigma_W\left(R_{sr} + R_{xy}\right) f_p(\psi_s)\frac{dW_s}{dt}\right]\left[1 + \sigma_W W_s\left(R_{sr} + R_{xy}\right)\frac{df_p(\psi_s)}{d\psi_s}\right]^{-1}, \\
\frac{d\psi_r}{dt} &= -A\frac{dR_{sr}}{dt} - \sigma_W R_{sr}\left[f_p(\psi_s)\frac{dW_s}{dt} + W_s\frac{df_p(\psi_s)}{d\psi_s}\frac{d\psi_s}{dt}\right],
\end{aligned} \tag{13}$$

with

$$\begin{aligned}
\frac{df_p(\psi_s)}{d\psi_s} &= -\frac{n\,K_p^n\,\psi_s^{n-1}}{(K_p^n + \psi_s^n)^2}, \\
\frac{dR_{sr}}{dt} &= -\frac{r_{sr}\,\alpha_r}{W_r^{(1+\alpha_r)}}\frac{dW_r}{dt}, \\
\frac{dR_{xy}}{dt} &= -\left[\frac{r_{xy,s}\,\alpha_s}{W_s^{(1+\alpha_s)}}\frac{dW_s}{dt} + \frac{r_{xy,r}\,\alpha_r}{W_r^{(1+\alpha_r)}}\frac{dW_r}{dt}\right] && \text{without nematodes,} \\
\frac{dR_{xy}}{dt} &= -\left[\frac{r_{xy,s}\,\alpha_s}{W_s^{(1+\alpha_s)}}\frac{dW_s}{dt} + \frac{r_{xy,r}\,\alpha_r}{W_r^{(1+\alpha_r)}}\frac{dW_r}{dt}\frac{\phi\,W_g}{W_g + W_r}\right] \\
&\quad + \frac{r_{xy,r}\,\phi}{W_r^{\alpha_r}}\left[\frac{(W_g + W_r)\frac{dW_g}{dt} - W_g\left(\frac{dW_g}{dt} + \frac{dW_r}{dt}\right)}{(W_g + W_r)^2}\right] && \text{with nematodes.}
\end{aligned}$$

A.2 Carbon transport modelling

To represent carbon transport through phloem vessels, we use a transport-resistance model with one source, the shoots (index s), and two sinks, the roots (index r) and fruits (index f) (Minchin et al., 1993; Thornley and Johnson, 1990), as illustrated in Figure A.13.

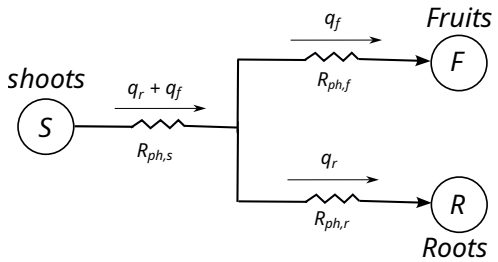

Figure A.13: Diagram of carbon transport from shoots to roots and fruits. Phloem flow rates (q) depend on phloem resistances (R_{ph}).

Sap flows within phloem vessels along carbon concentration gradients, so Figure A.13 trans-

lates into the following equations:

$$\begin{aligned}(q_r + q_f)R_{ph,s} + q_f R_{ph,f} &= (C_s - C_f),\\ (q_r + q_f)R_{ph,s} + q_r R_{ph,r} &= (C_s - C_r),\end{aligned} \tag{14}$$

where q_x are the phloem flow rates and $R_{ph,x}$ the phloem resistances associated to the different plant compartments, defined as follows:

$$R_{ph,s} = \frac{r_{ph,s}}{W_s^{\alpha_s}}, \quad R_{ph,r} = \frac{r_{ph,r}}{(W_r + W_g)^{\alpha_r}}, \quad R_{ph,f} = \frac{r_{ph,f}}{W_f^{\alpha_f}}.$$

We assume that carbon transport in phloem vessels is affected by the presence of galls (W_g): reducing the phloem resistance in the roots, they accelerate the carbon flow to the roots.

Solving for q_r and q_f from (14) gives:

$$\begin{aligned}q_r &= \frac{1}{\Delta}(R_{ph,f}(C_s - C_r) + R_{ph,s}(C_f - C_r)),\\ q_f &= \frac{1}{\Delta}(R_{ph,r}(C_s - C_f) + R_{ph,s}(C_r - C_f)),\\ \text{with: } \Delta &= R_{ph,f}(R_{ph,s} + R_{ph,r}) + R_{ph,s}\,R_{ph,r}.\end{aligned}$$

Therefore, the carbon transport fluxes from shoots to roots (T_r) and shoots to fruits (T_f) are:

$$\begin{aligned}T_r = q_r C_s &= \frac{C_s}{\Delta}(R_{ph,f}(C_s - C_r) + R_{ph,s}(C_f - C_r)),\\ T_f = q_f C_s &= \frac{C_s}{\Delta}(R_{ph,r}(C_s - C_f) + R_{ph,s}(C_r - C_f)).\end{aligned} \tag{15}$$

As described in Section 2.1, to account for the vegetative-reproductive transition, instead of using a step function, we introduced the hill function $M(W_s)$ (3) wisely in the transport term T_r in equation (15):

$$\begin{aligned}T_r &= \frac{C_s}{\Delta_r}(R_{ph,f}(C_s - C_r) + M(W_s) \times R_{ph,s}(C_f - C_r)),\\ T_f &= M(W_s)\left[\frac{C_s}{\Delta}(R_{ph,r}(C_s - C_f) + R_{ph,s}(C_r - C_f))\right],\\ \text{with: } \Delta_r &= R_{ph,f}(R_{ph,s} + R_{ph,r}) + M(W_s) \times R_{ph,s}\,R_{ph,r}.\end{aligned} \tag{16}$$

So, from equation (16), at the vegetative stage which corresponds to ($M(W_s) \approx 0$), meaning that plant is not yet mature to provide fruits. The configuration of carbon transport presented in Figure A.13 simplifies to a 1-source 1-sink system (shoots to roots). In that case, the transport of carbon from shoots to roots is given by: $T_r = \frac{C_s}{R_{ph}}(C_s - C_r)$, with $R_{ph} = R_{ph,s} + R_{ph,r}$ (Minchin et al., 1993).

In conclusion, to describe the carbon allocation in a single approach for both vegetative and reproductive stages, we consider the transport terms in equation (16).

Moreover, during the reproductive stage, additional carbon is pumped by fruits for their ripening process (Colombié et al., 2017). So, we considered an active transport term as follows:

$$T_a = M(W_s)\left[t_a\left(\frac{C_s}{K_a + C_s}\right)\left(\frac{K_i}{K_i + C_f}\right)W_f\right], \tag{17}$$

where t_a is active transport rate, K_a and K_i are half-saturation constants for shoot carbon supply and fruit carbon inhibition, respectively. This formulation accounts for saturation at high shoot carbon levels, and includes an inhibitory effect of C_f, which limits flux when fruits already contain abundant carbon. Such an active transport mechanism, as highlighted by Fishman and Génard (1998), provides a realistic description of the dominant sink strength of fruits.

B Experimental data

Table 5: Experimental data (Jauzion-Graverolle et al., 2025): weekly number of leaves for the healthy control plants.

Crop	Week											
	1	2	3	4	5	6	7	8	9	10	11	12
Tomato	4.12	8.18	12.1	14.7	16.16	17.35	19.01	21.24	23.92	26.63	29.27	31.86
Pepper	4.27	10.71	19.48	30.74	41.67	49.16	53.34	54.72	54.64	54.53	53.83	52.72

Mean values over 6 replicates

Table 6: Experimental data (Jauzion-Graverolle et al., 2025): plant dry masses for shoots (W_s), roots (W_r), and fruits (W_f).

Crop	Variable	Treatment	Value* (in grams)		
			t_0	$t_0 + 6$ weeks	$t_0 + 12$ weeks
Tomato	W_s	control	0.25 ± 0.08	16.04 ± 3.2	26.27 ± 4.36
		inoculated		14.25 ± 1.01	14.29 ± 3.74
	W_r	control	0.06 ± 0.02	1.75 ± 0.67	1.64 ± 0.34
		inoculated		1.93 ± 0.13	4.35 ± 1.17
	W_f	control	0	–	3.07 ± 2.96
		inoculated		–	0.44 ± 0.98
Pepper	W_s	control	0.11 ± 0.03	6.9 ± 0.76	7.67 ± 0.51
		inoculated		5.8 ± 0.84	7.12 ± 0.71
	W_r	control	0.03 ± 0.01	2.11 ± 0.65	1.19 ± 0.11
		inoculated		0.85 ± 0.19	1.85 ± 0.26
	W_f	control	0	1.03 ± 0.43	9.5 ± 0.83
		inoculated		0.51 ± 0.28	8.48 ± 1.6

*Mean value $\pm$ standard deviation over 6 replicates

Table 7: Experimental data (Jauzion-Graverolle et al., 2025): RKN measures.

Variable	Crop	Value*	
		$t_0 + 6$ weeks	$t_0 + 12$ weeks
Number of egg masses (F)	tomato	2282 ± 253	548 ± 273
	pepper	635 ± 511	1932 ± 468
Number of eggs per egg masses (ρ/μ_F)	tomato	328 ± 80	232 ± 15
	pepper	319.79 ± 96	312.5 ± 76
Number of juvenile larvae (J_2)	tomato	–	207787 ± 142251
	pepper		83413 ± 57649
Number of galls ($G \approx \xi J + F$)	tomato	3283 ± 365	–
	pepper	1304 ± 538	

*Mean value ± standard deviation over 6 replicates

Note: At time (t_0+12), the roots were severely invaded by galls, making counting impossible.

C Appendix: Setting parameter values

This section describes how the parameters were set, outside the estimation procedure described in Section 3.2.

C.1 Leaf–biomass allometry

In order to use the leaf count data in the calibration procedure, we fit an allometric relationship between shoot dry mass (W_s) and number of leaves (L_f) (Le Maitre and Midgley, 1991; Zeinali et al., 2014), given by:

$$W_s^{\text{leaf}} = a\ L_f^b. \tag{18}$$

Coefficient a was estimated separately for each crop species, whereas allometric exponent b was estimated jointly for both.

Before applying this relationship, the leaf measurements were pre-processed to ensure consistency and reliability. The procedure involved cleaning and smoothing to reduce irregularities, outliers, and measurement noise in the raw data for each species. This was achieved using the `make_smoothing_spline` Python function.

We used the `differential_evolution` method (Python, SciPy v1.11) to minimise the sum of squared errors on the dry masses. The estimation results are shown in Section C.1.

C.2 Parameter simplifications for the plant model

For the calibration procedure, we simplified the parameterisation of the plant model (1,13).

For several plant traits, we found no information specific to the three plant compartments (shoots, roots, and fruits), so we decided to take the same parameter value across compartments. This concerned: the xylem resistance coefficients set to r_{xy} (no parameter for the fruit compartment); the maintenance rates set to m; the respiration rates set to v; the allometric coefficients set to α. The shoot and root phloem resistance coefficients were set to r_{ph}.

To represent the fruit priority for carbon resources, we set fruit parameter values relatively

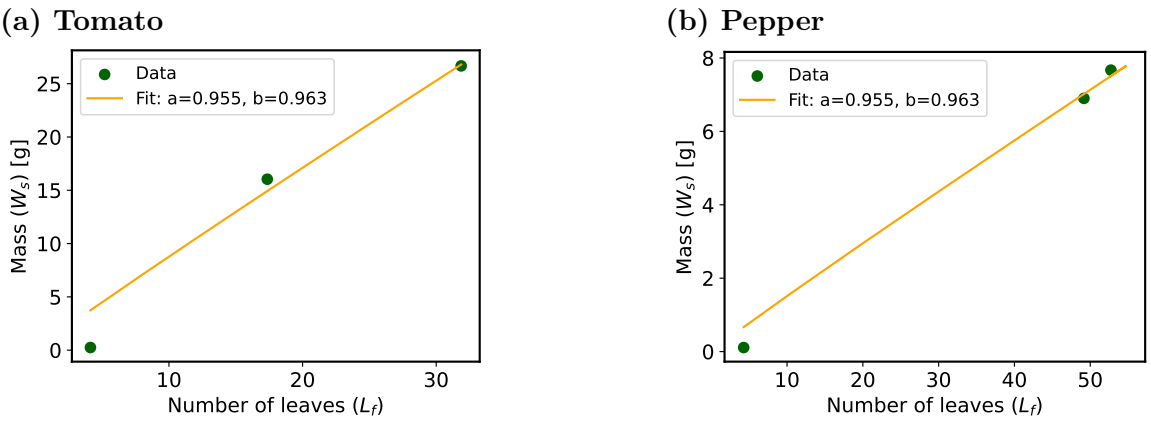

Figure C.14: Estimation of leaf–biomass allometric coefficients based on equation (18). Allometric exponent b is estimated jointly for both crop species.

to shoot values as follows: for the phloem resistance coefficient $r_{ph,f} = r_{ph}/2$ and for the half-saturation constant for growth of the fruit $K_f = K_s/2$.

Thanks to these assumptions, the 38 parameters of the plant model were reduced to 28 parameters.

C.3 Parameter setting before the sensitivity analysis

To choose the plant parameters to be estimated, we performed a sensitivity analysis described in Section 3.2.1.

After reducing the number of plant parameters to 28, as detailed in Section C.2, we made an extra simplification on the half-saturation constants for water effect on photosynthesis (K_p) and growth (K_k), by setting the difference between the two: $K_p = K_k - 200$ kPa. This allowed to maintain the order between the two, as water stress first affects photosynthesis.

Moreover, we excluded three parameters from the sensitivity analysis and set their values as follows. The Hill coefficient intervening in the water-stress functions (2) was arbitrarily set to $n = 6$, which corresponds to fairly stiff switch-like functions. As we found no specific information on the rhizodeposition rate (z) and the soil water potential (ψ_{soil}), we set both parameters according to Dewar (1993). Values can be found in Table 1.

Therefore, the sensitivity analysis was based on only 24 plant parameters, identified in Table 8. The levels used in the analysis were determined within literature-based ranges.

C.4 Sensitivity analysis on the healthy plant dynamics

To determine which physiological processes exert the strongest control over plant growth, we performed a global sensitivity analysis on the healthy plant model, described in Section 3.2.1. Figure C.15 shows the results for three outputs, the dry masses of the different plant compartments. The results on the other state variables, the carbon concentrations and water potentials (not shown), did not provide additional information.

We defined a parameter as influential when its generalised sensitivity index (GSI) exceeded 5%. According to this criterion, eight parameters emerged as major contributors to model variability: the photosynthetic rate (p), the growth rate coefficients for shoots (k_s), roots (k_r), and fruits (k_f), the maintenance rate (m) and the transpiration rate (σ_W). These parameters

Table 8: Parameter levels used for the global sensitivity analysis on the plant model, prior to parameter estimation (Section C.4). Parameter units are indicated in Table 7

Parameter	Description	Levels
p	Photosynthesis rate[3]	(0.1, 0.6, 0.9)
σ_W	Shoot transpiration rate[‡]	(5, 13, 40)
r_{ph}	Phloem resistance coefficient[3]	$(3 \cdot 10^{-2}, 0.1, 0.5)$
r_{xy}	Xylem resistance coefficient[‡]	$(2, 5, 8)$
r_{sr}	Root water uptake resistance[7]	$(0.2, 1, 3)$
k_s, k_r, k_f	Biomass growth rates[3,8]	$(0.1, 0.5, 0.9)$
K_s, K_r	Half-saturation constants for growth[3]	$(5 \cdot 10^{-3}, 2 \cdot 10^{-2}, 0.1)$
d_s, d_f	Mortality rates[3]	$(1/80, 1/50, 1/30)$
d_r	Root mortality rate[6]	$(1/300, 1/200, 1/75)$
ψ_{soil}	Water potential of soil[7]	-100
n	Hill coefficient[0]	6
W_{onset}	Threshold shoot biomass for fruit onset[†]	$(2, 10, 20)$
K_k	Half-saturation constant for water effect on growth[1]	$(-1600, -1400, -1200)$
K_p	Half-saturation constant for water effect on photosynthesis	K_k - 200
c	Carbon fraction of structural dry matter[2]	0.45
α	Allometric coefficient for growth[†]	$(1/3, 2/3, 1)$
m	Maintenance respiration rate[3]	$(10^{-3}, 10^{-2}, 5 \cdot 10^{-2})$
v	Growth respiration rate[5]	$(10^{-2}, 0.1, 0.2)$
z	Rhizodeposition rate[7]	$(2 \cdot 10^{-2}, 0.1, 0.5)$
t_a	Active transport rate[4]	$(2 \cdot 10^{-2}, 0.1, 0.5)$
K_m	Half-saturation constant for maintenance[3]	$(5 \cdot 10^{-4}, 2 \cdot 10^{-3}, 10^{-2})$
K_u	Half-saturation constant for self-shading[0]	$(2, 7, 14)$
K_a	Half-saturation constant for active transport[4]	$(2 \cdot 10^{-2}, 0.1, 0.5)$
K_i	Half-saturation constant for fruit inhibition[0]	$(5 \cdot 10^{-2}, 0.2, 0.5)$

Sources: [†]estimated from data (Jauzion-Graverolle et al., 2025) and [‡]computed in Section C.5.1; [0]assumed; [1](Weng, 2000; Delfine et al., 2002); [2](Li, 2007); [3](Brugge, 1985); [4](Liu et al., 2007); [5](Thornley and Cannell, 2000); [6](Wang et al., 2024); [7](Dewar, 1993); [8](Gerlin et al., 2022).

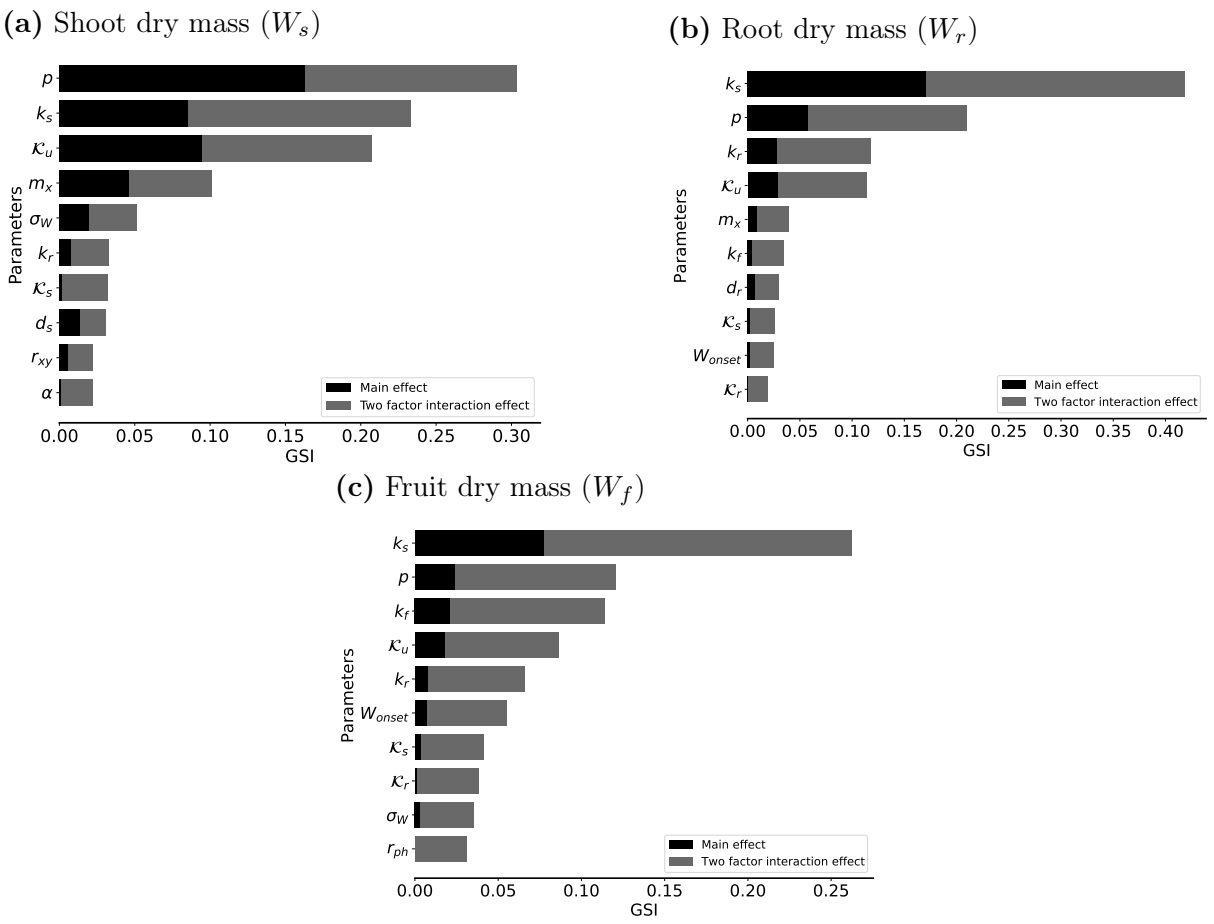

Figure C.15: Global sensitivity analysis on the healthy plant model (1,13). Parameter main (black bars) and two-way interaction (grey bars) effects on the plant dry masses. Only the 10 most influential parameters are represented. All parameter levels are listed in Table 8.

govern core physiological processes, namely carbon acquisition, biomass growth and maintenance. In addition to these primary drivers, two other parameters also displayed notable influence: the self-shading constant (K_u) and the threshold shoot biomass for fruit onset (W_{onset}).

Among these eight influential parameters, one could be directly set from data (W_{onset}), (σ_W) computed in Section C.5.1, and two from the literature (K_u and m). That left four influential parameters to be estimated: p, k_s, k_r, and k_f.

C.5 Parameter setting before the estimation procedure

C.5.1 Healthy plant model

After simplifications described in Section C.2, there were 28 plant parameters. Based on the sensitivity analysis results in Section C.4, 4 highly influential parameters were retained for the estimation procedure (p, k_r, k_s, k_f), plus 2 for which we found little information in the literature (t_a, r_{ph}). For the remaining 22 parameters, 4 were derived from experimental data (directly for W_{onset} and see paragraphs below for the other 3) and 18 were set from the literature. Among these 18 parameters, 3 were crop-specific (d_r, K_k, K_p) and 15 were generic, the latter including the 3 parameters fixed in the sensitivity analysis (n, z, ψ_{soil}). All the plant parameter information and values are summarised in Table 1.

Xylem resistance coefficient r_{xy} and allometry coefficient α We estimated these two parameters jointly for tomato and pepper, combining healthy and infested plant data (Jauzion-Graverolle et al., 2025), based on the allometric relationship linking hydraulic conductance L and shoot dry mass W:

$$L = aW^{\alpha}, \quad \text{with} \quad r_{xy} = \frac{1}{a}. \tag{19}$$

We used the `differential_evolution` method (Python, SciPy v1.11) to minimise the sum of squared errors on the hydraulic conductance. Results are illustrated in Figure C.16 and resulting parameter values reported in Table 1.

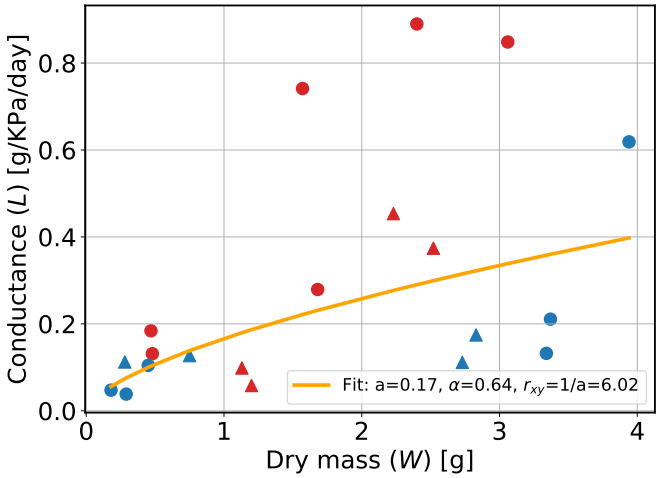

Figure C.16: Calibration of the allometric relationship between hydraulic conductance (L) and dry mass (W) relationship based on equation (19). All data are pooled: tomato (red) and pepper (blue), healthy plants (triangles) and infested plants (circles).

Transpiration rate σ_W The transpiration rate measured in Jauzion-Graverolle et al. (2025) was $A_{\text{sec}} = 1\text{mmol} \cdot \text{m}^{-2} \cdot \text{s}^{-1}$. To extrapolate this value to a daily transpiration rate, it is necessary to account for the day length. Indeed, transpiration occurs essentially during daytime and is (almost) zero at night (Rice et al., 2017). The experiment took place between February and May, so considering approximately 10 hours of light per day, we obtain:

$$\begin{aligned} A_{\text{day}} &= 1 \times 10 \times 3600 \text{ mmol} \cdot \text{m}^{-2} \cdot \text{day}^{-1} \\ &= 18 \cdot 10^{-3} \times 10 \times 3600 \text{ g}_{\text{H}_2\text{O}} \cdot \text{m}^{-2} \cdot \text{day}^{-1} = 648 \text{ g}_{\text{H}_2\text{O}} \cdot \text{m}^{-2} \cdot \text{day}^{-1} \end{aligned}$$

Specific leaf area (SLA) To convert transpiration rate per square meter to a rate per gram of leaf dry mass, we must account for the leaf density (surface-to-weight ratio), expressed as SLA. According to Jauzion-Graverolle et al. (2025), the SLA remains relatively constant across species and treatments: $SLA \approx 250\,\text{cm}^2/\text{g} = 2.5 \cdot 10^{-2}$ m^2/g. Thus, the transpiration rate per unit of leaf biomass per day is:

$$\sigma_{W_0} = 648 \times 2.5 \cdot 10^{-2} = 16 \text{ g}_{\text{H}_2\text{O}} \cdot \text{g}^{-1} \cdot \text{day}^{-1}.$$

Excluding stem contribution In our model, shoot transpiration is $A = \sigma_W W_s f_p(\psi_s)$ (11), where W_s denotes the shoot biomass, which includes leaves and stems. In practice, stems do not contribute significantly to transpiration (although they contribute slightly to photosynthesis).

The fraction of biomass allocated to stems varies with plant development and species (Poorter et al., 2012). Assuming a constant stem fraction $st = 20\%$ of shoot biomass, the transpiration rate becomes:

$$A = [\sigma_{W_0}(1 - st)]\, W_s\, f_p(\psi_s), \quad \text{with} \quad \sigma_W = \sigma_{W_0} \times (1 - 0.2) \approx 13 \text{ day}^{-1}.$$

C.5.2 Coupled model

There are 18 extra parameters in the coupled model, in addition to the plant parameters.

We first assumed that the half-saturation constants for feeding and reproduction were equal, $K_\gamma = K_\rho$, as both processes are linked. We also linked the half-saturation constants for gall formation and root growth as follows: $K_g = K_r/10$, to favour galls over plant growth for carbon resource, as RKN are efficient parasites.

Among the remaining 16 parameters, 3 were directly derived from data ($\rho_{\min}, \rho_{\max}, \phi$), 2 were computed from expert knowledge (see below), and 6 were set from the literature (λ, μ_e). The remaining 5 parameters were estimated (β, γ, k_g, K_ρ, K_ω). In the estimation procedure, we imposed that the half-saturation constant for establishment was smaller than for reproduction, $K_\omega \leq K_\rho$, as we assumed that carbon shortage in the plant would first affect nematode establishment.

The interaction and nematode parameter information and values are summarised in Table 1 and Table 2, respectively.

Estimation of λ and μ_e On average, the RKN egg hatching rate is around 46% and eggs typically remain in the soil for approximately two weeks. In the model, this translates as follows:

- proportion of eggs hat become juvenile larvae J_2: $\frac{\lambda}{\lambda+\mu_E} = 0.46$,

- average residence time in the egg stage E: $\frac{1}{\lambda+\mu_E} = 13$ days.

So, $\lambda = \frac{0.46}{13}$ day^{-1} and $\mu_E = \frac{0.54}{13}$ day^{-1}.

D Additional illustrations of plant–RKN dynamics

D.1 Healthy plant dynamics

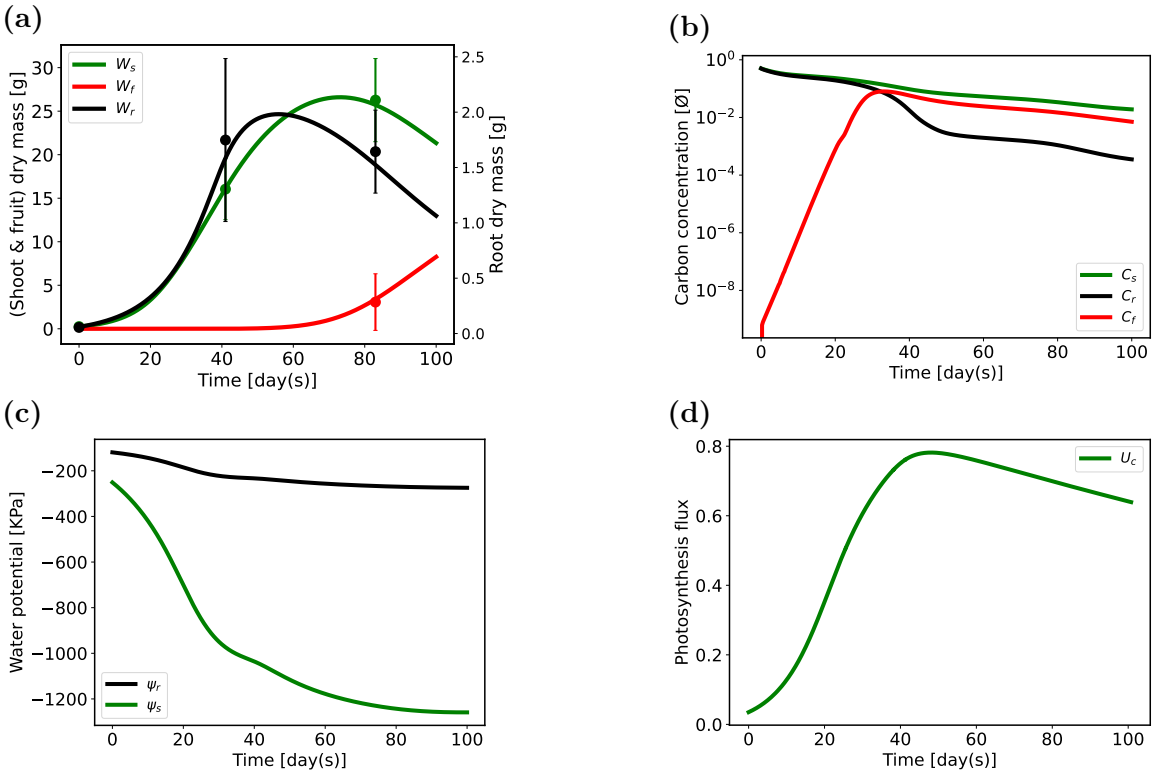

Figure D.17: Healthy tomato dynamics, according to system (1,13), with initial conditions defined in Section 3.3: (a) dry masses (W_x) for shoots ($x = s$), roots ($x = r$) and fruits ($x = f$), with corresponding data points (mean and standard deviations); (b) carbon concentrations (C_x); (c) water potentials (ψ_x); (d) photosynthesis flux (U_c). Parameter values are given in Table 1.

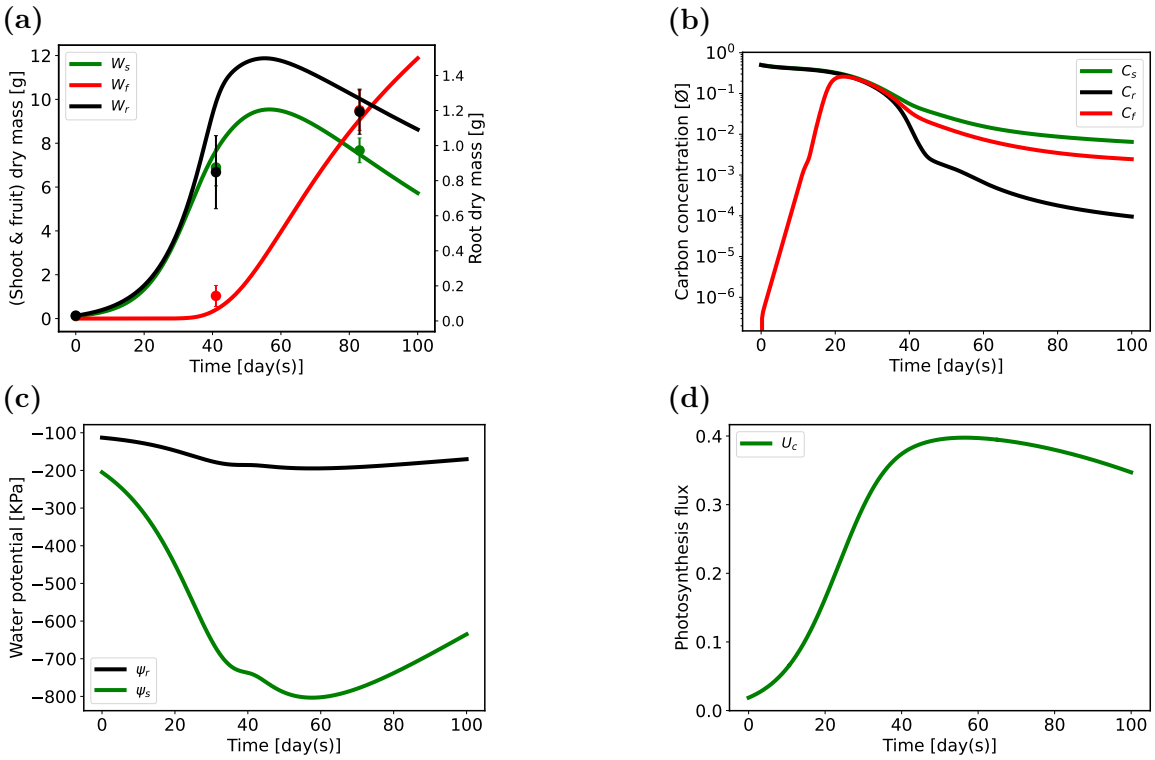

Figure D.18: Healthy pepper dynamics, according to system (1,13), with initial conditions defined in Section 3.3: (a) dry masses (W_x) for shoots ($x = s$), roots ($x = r$) and fruits ($x = f$), with corresponding data points (mean and standard deviations); (b) carbon concentrations (C_x); (c) water potentials (ψ_x); (d) photosynthesis flux (U_c). Parameter values are given in Table 1, data in Table 6.

D.2 Infested plant dynamics

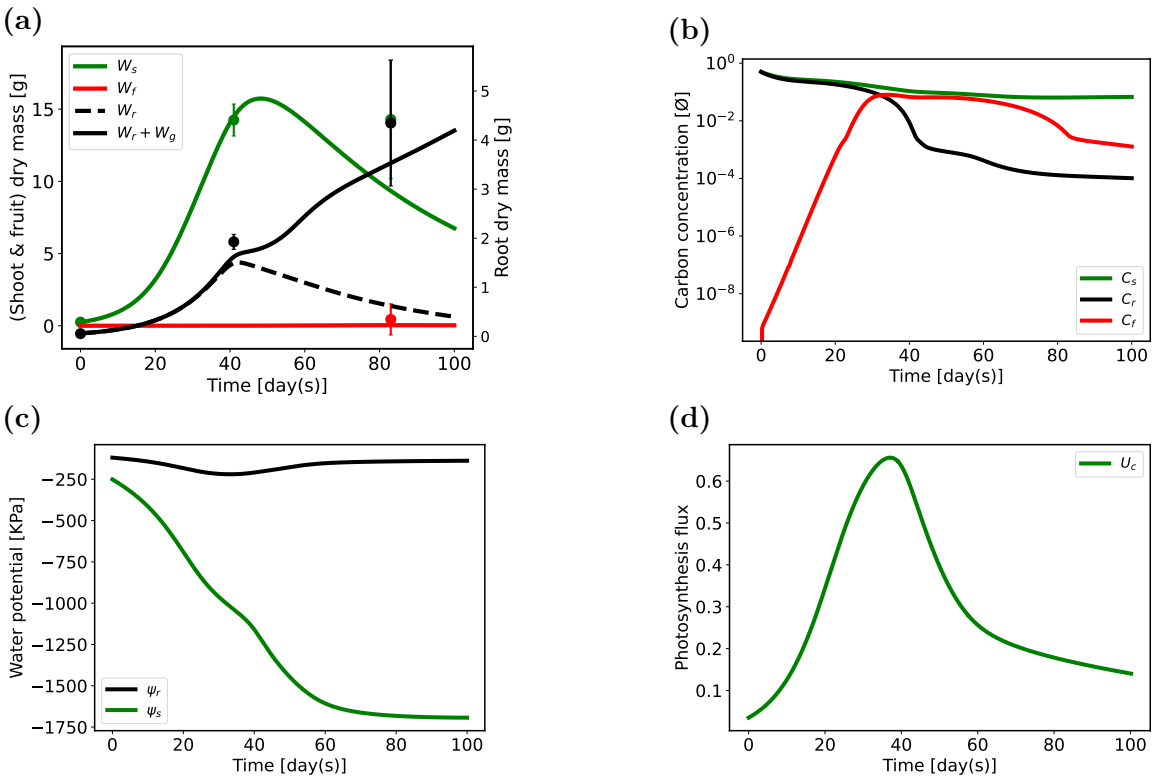

Figure D.19: Infested tomato dynamics, according to system (1,13,4,6), with initial conditions defined in Section 3.3: (a) dry masses (W_x) for shoots ($x = s$), roots ($x = r$) and fruits ($x = f$), with corresponding data points (mean and standard deviations); (b) carbon concentrations (C_x); (c) water potentials (ψ_x); (d) photosynthesis flux (U_c). Parameter values are given in Table 1 and Table 2, data in Table 6 and Table 7.

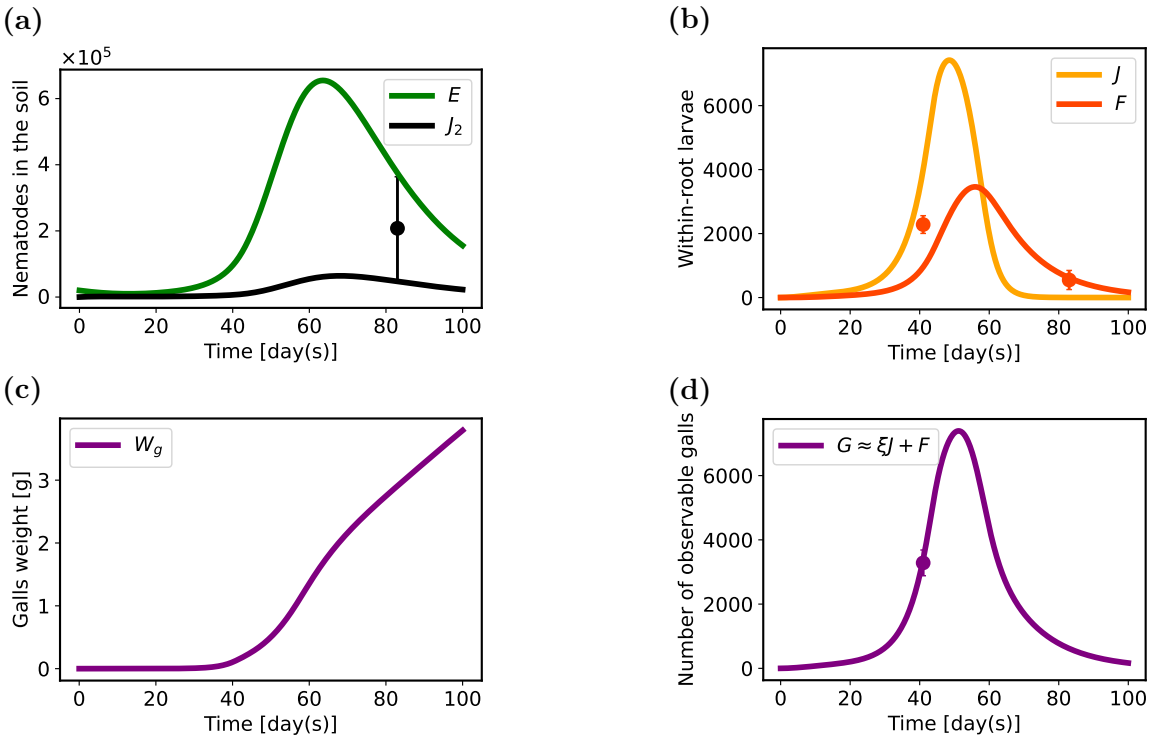

Figure D.20: Nematode dynamics in tomato, according to system (1,13,4,6), with initial conditions defined in Section 3.3: (a) free-living stages, eggs (E) and juvenile larvae (J_2); (b) within-root stages, infesting larvae (J) and mature females (F); (c) gall biomass (W_g); (d) number of galls (G). Parameter values are given in Table 1 and Table 2, data in Table 6 and Table 7.

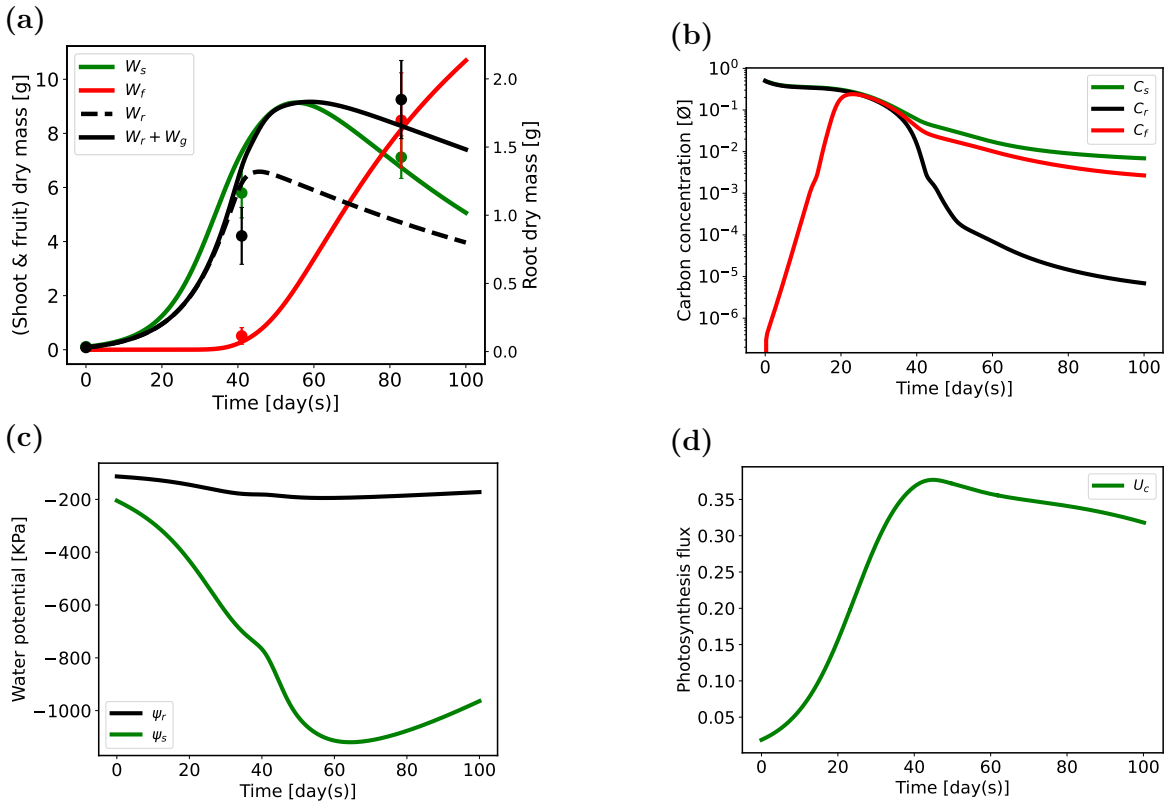

Figure D.21: Infested pepper dynamics, according to system (1,13,4,6), with initial conditions defined in Section 3.3: (a) dry masses (W_x) for shoots ($x = s$), roots ($x = r$) and fruits ($x = f$), with corresponding data points (mean and standard deviations); (b) carbon concentrations (C_x); (c) water potentials (ψ_x); (d) photosynthesis flux (U_c). Parameter values are given in Table 1 and Table 2, data in Table 6 and Table 7.

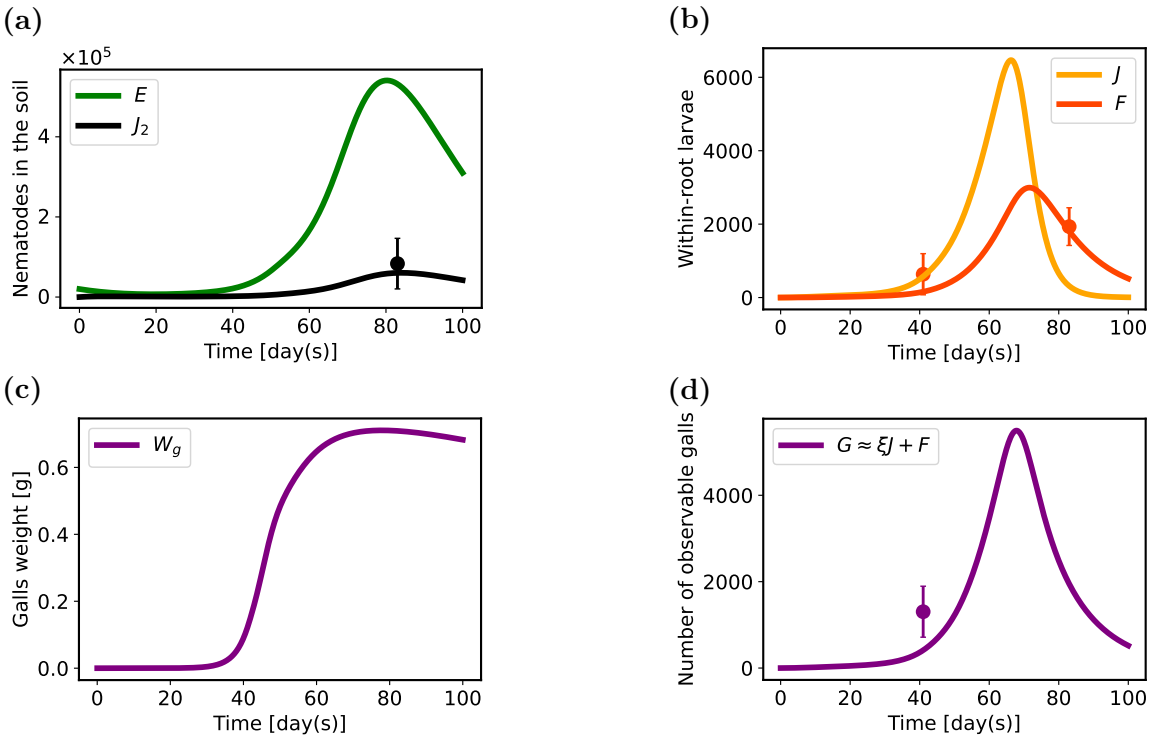

Figure D.22: Nematode dynamics in pepper, according to system (1,13,4,6), with initial conditions defined in Section 3.3: (a) free-living stages, eggs (E) and juvenile larvae (J_2); (b) within-root stages, infesting larvae (J) and mature females (F); (c) gall biomass (W_g); (d) number of galls (G). Parameter values are given in Table 1 and Table 2, data in Table 6 and Table 7.

D.3 Plant growth responses to self-shading and water stress

Environmental scenario simulations were conducted on the plant model to evaluate growth sensitivity under abiotic constraints. Two types of stress were simulated. First, shading, implemented by reducing the photosynthesis rate p by half at $t = 25$ days. Second, water stress, represented by doubling the soil-root resistance r_{sr} relative to its reference value, also at $t = 25$ days.

The results are consistent with observed plant responses. Under shading (Figure D.23), aboveground growth is favored over root growth, resulting in an increased shoot:root ratio. This response reflects the reduced photosynthetic activity and, consequently, the limited carbon availability, with priority allocation to shoots. Additionally, a longer transitional period from the vegetative to the reproductive phase is observed compared with the unshaded scenario.

In contrast, under water stress (Figure D.24), the plant reallocates resources to favor root growth at the expense of aboveground biomass. The decrease in the shoot:root ratio reflects this adaptive strategy, aimed at enhancing soil exploration and water uptake under limiting conditions. However, this reallocation comes at the cost of slower shoot growth, highlighting the physiological trade-off imposed by water limitation.

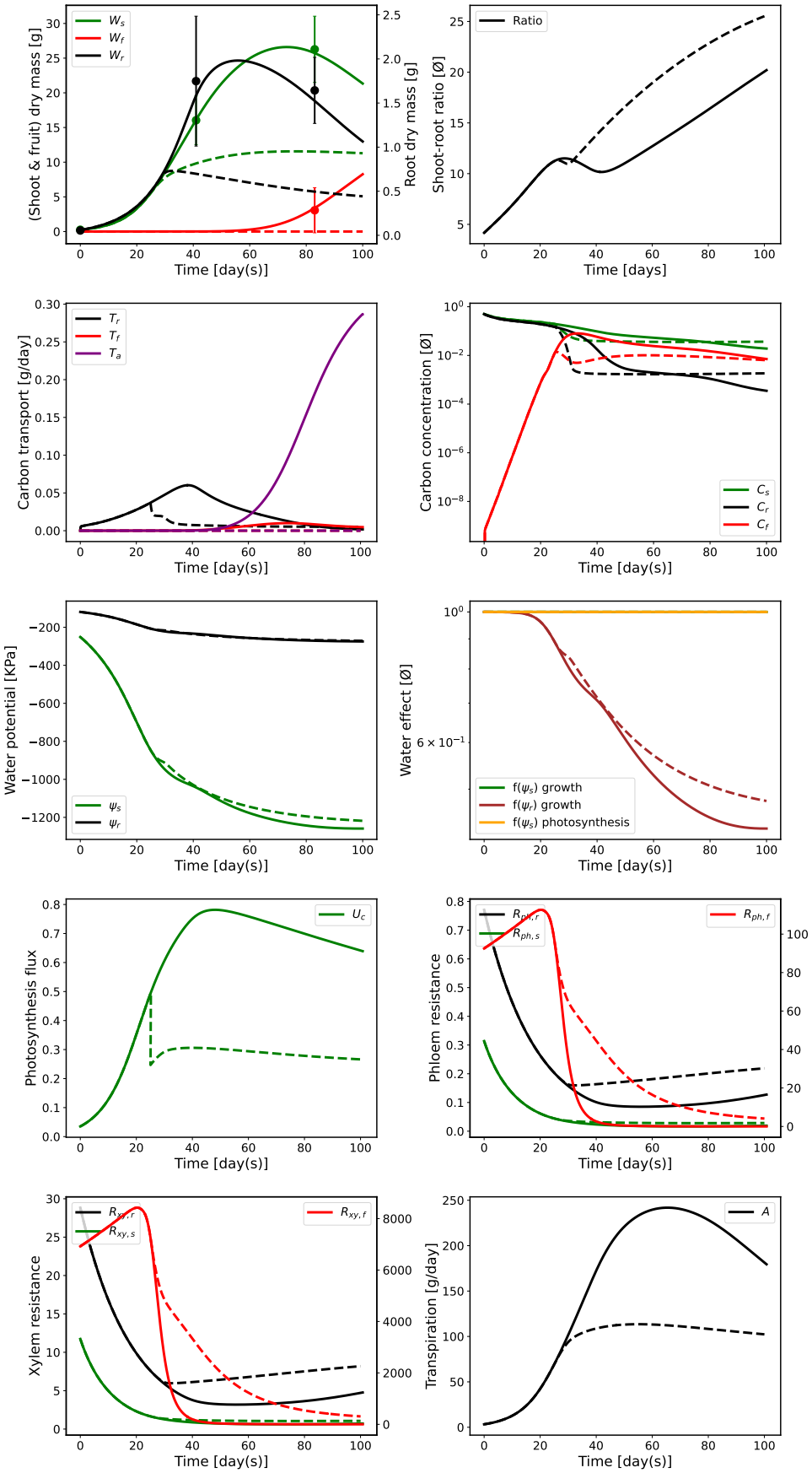

Figure D.23: Healthy plant dynamics under normal conditions (solid lines) and under shading (dashed lines). The stress scenario is applied at 25 days. Model parameters are listed in Table 1.

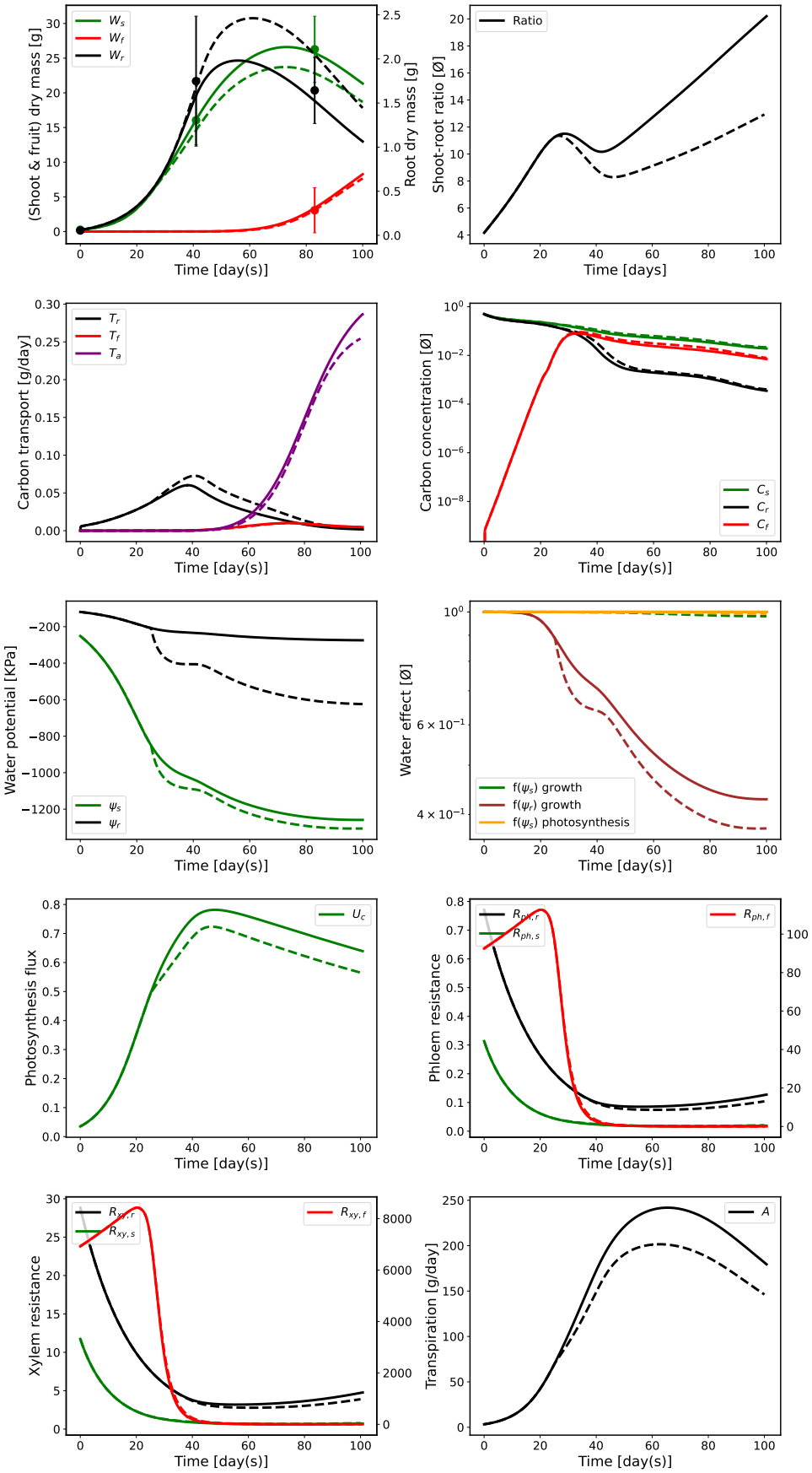

Figure D.24: Healthy plant dynamics under normal conditions (solid lines) and under water stress (dashed lines). The stress scenario is applied at 25 days. Model parameters are listed in Table 1.

References

Aggarwal, P.K., Kalra, N., Chander, S., Pathak, H., 2006. InfoCrop: a dynamic simulation model for the assessment of crop yields, losses due to pests, and environmental impact of agro-ecosystems in tropical environments. model description. Agricultural Systems 89, 1–25. doi:10.1016/j.agsy.2005.08.001.

Ajayi, A., 2020. Root-knot nematodes: a wake-up call to rescue crops in africa from *Meloidogyne incognita* and its allies, in: Journal of Agriculture and Veterinary Science, pp. 78–89.

Anwar, S.A., Mckenry, M., 2012. Incidence and population density of plant-parasitic nematodes infecting vegetable crops and associated yield losses in punjab, pakistan. Pakistan Journal of Zoology .

Barbary, A., Djian-Caporalino, C., Palloix, A., Castagnone-Sereno, P., 2015. Host genetic resistance to root-knot nematodes, *Meloidogyne* spp., in Solanaceae: from genes to the field. Pest Management Science 71, 1591–1598. doi:10.1002/ps.4091.

Barber, D.A., Martin, J.K., 1976. The release of organic substances by cereal roots into soil. New Phytologist 76, 69–80. doi:10.1111/j.1469-8137.1976.tb01439.x.

Berg, R.H., Fester, T., Taylor, C.G., 2009. Development of the root-knot nematode feeding cell, in: Berg, R.H., Taylor, C.G. (Eds.), Cell Biology of Plant Nematode Parasitism. Berlin, Heidelberg, pp. 115–152. doi:10.1007/978-3-540-85215-5_5.

Bishop, S.C., 2012. A consideration of resistance and tolerance for ruminant nematode infections. Frontiers in Genetics 3. doi:10.3389/fgene.2012.00168.

Brisson, N., Gary, C., Justes, E., Roche, R., Mary, B., Ripoche, D., Zimmer, D., Sierra, J., Bertuzzi, P., Burger, P., Bussière, F., Cabidoche, Y.M., Cellier, P., Debaeke, P., Gaudillère, J.P., Hénault, C., Maraux, F., Seguin, B., Sinoquet, H., 2003. An overview of the crop model stics. European Journal of Agronomy 18, 309–332. doi:10.1016/S1161-0301(02)00110-7.

Brugge, R., 1985. A mechanistic model of grass root growth and development dependent upon photosynthesis and nitrogen uptake. Journal of Theoretical Biology 116, 443–467. doi:10.1016/S0022-5193(85)80281-2.

Cabrera, J., Díaz-Manzano, F.E., Barcala, M., Arganda-Carreras, I., de Almeida-Engler, J., Engler, G., Fenoll, C., Escobar, C., 2015. Phenotyping nematode feeding sites: three-dimensional reconstruction and volumetric measurements of giant cells induced by root-knot nematodes in Arabidopsis. The New Phytologist 206, 868–880. doi:10.1111/nph.13249.

Castagnone-Sereno, P., Bongiovanni, M., Dalmasso, A., 1992. Differential expression of root-knot nematode resistance genes in tomato and pepper: evidence with *Meloidogyne incognita* virulent and avirulent near-isogenic lineages. Annals of Applied Biology 120, 487–492. doi:10.1111/j.1744-7348.1992.tb04908.x.

Colombié, S., Beauvoit, B., Nazaret, C., Bénard, C., Vercambre, G., Le Gall, S., Biais, B., Cabasson, C., Maucourt, M., Bernillon, S., Moing, A., Dieuaide-Noubhani, M., Mazat, J.P., Gibon, Y., 2017. Respiration climacteric in tomato fruits elucidated by constraint-based modelling. New Phytologist 213, 1726–1739. doi:10.1111/nph.14301.

Cook, C.G., Robinson, A.F., Namken, L.N., 1997. Tolerance to rotylenchulus reniformis and resistance to meloidogyne incognita race 3 in high-yielding breeding lines of upland cotton. Journal of Nematology 29, 322–328.

Cook, D.E., Lee, T.G., Guo, X., Melito, S., Wang, K., Bayless, A.M., Wang, J., Hughes, T.J., Willis, D.K., Clemente, T.E., Diers, B.W., Jiang, J., Hudson, M.E., Bent, A.F., 2012. Copy number variation of multiple genes at *Rhg1* mediates nematode resistance in soybean. Science 338, 1206–1209. doi:10.1126/science.1228746.

Cunniffe, N.J., Gilligan, C.A., 2011. A theoretical framework for biological control of soil-borne plant pathogens: identifying effective strategies. Journal of Theoretical Biology 278, 32–43. doi:10.1016/j.jtbi.2011.02.023.

Delfine, S., Tognetti, R., Loreto, F., Alvino, A., 2002. Physiological and growth responses to water stress in field-grown bell pepper (*Capsicum annuum*). The Journal of Horticultural Science and Biotechnology 77, 697–704. doi:10.1080/14620316.2002.11511559.

Dewar, R.C., 1993. A root-shoot partitioning model based on carbon-nitrogen-water interactions and munch phloem flow. Functional Ecology 7, 356–368. doi:10.2307/2390216.

Dietze, M.C., Matthes, J.H., 2014. A general ecophysiological framework for modelling the impact of pests and pathogens on forest ecosystems. Ecology Letters 17, 1418–1426. doi:10.1111/ele.12345.

Djian-Caporalino, C., Fazari, A., Arguel, M.J., Vernie, T., VandeCasteele, C., Faure, I., Brunoud, G., Pijarowski, L., Palloix, A., Lefebvre, V., Abad, P., 2007. Root-knot nematode (*Meloidogyne spp.*) me resistance genes in pepper (*Capsicum annuum L.*) are clustered on the p9 chromosome. Theoretical and Applied Genetics 114, 473–486. doi:10.1007/s00122-006-0447-3.

Djian-Caporalino, C., Molinari, S., Palloix, A., Ciancio, A., Fazari, A., Marteu, N., Ris, N., Castagnone-Sereno, P., 2011. The reproductive potential of the root-knot nematode *Meloidogyne incognita* is affected by selection for virulence against major resistance genes from tomato and pepper. European Journal of Plant Pathology 131, 431–440. doi:10.1007/s10658-011-9820-4.

Dorhout, R., 1991. Water transport through tomato roots infected with *Meloidogyne incognita*. Phytopathology 81, 379. doi:10.1094/Phyto-81-379.

Downton, W., 1977. Photosynthesis in salt-stressed grapevines. Functional Plant Biology 4, 183. doi:10.1071/PP9770183.

Fishman, S., Génard, M., 1998. A biophysical model of fruit growth: simulation of seasonal and diurnal dynamics of mass. Plant, Cell & Environment 21, 739–752. doi:10.1046/j.1365-3040.1998.00322.x.

Gerlin, L., Cottret, L., Escourrou, A., Genin, S., Baroukh, C., 2022. A multi-organ metabolic model of tomato predicts plant responses to nutritional and genetic perturbations. Plant Physiology 188, 1709–1723. doi:10.1093/plphys/kiab548.

Hallmann, J., Meressa, B.H., 2018. Nematode parasites of vegetables, in: Plant parasitic nematodes in subtropical and tropical agriculture. CABI Books, pp. 346–410. doi:10.1079/9781786391247.0346.

Jammes, F., Lecomte, P., de Almeida-Engler, J., Bitton, F., Martin-Magniette, M.L., Renou, J.P., Abad, P., Favery, B., 2005. Genome-wide expression profiling of the host response to root-knot nematode infection in arabidopsis. The Plant Journal 44, 447–458. doi:10.1111/j.1365-313X.2005.02532.x.

Jauzion-Graverolle, N., Caravel, C., Doussan, C., Faubert, P., Jaubert, S., Pagès, L., Serra, V., Touzeau, S., Baldazzi, V., Djian-Caporalino, C., 2025. Inter-species variability of root-knot nematode infection dynamics through the simultaneous monitoring of both pathogen and host development. URL: https://hal.inrae.fr/hal-05397476. HAL preprint.

Jones, J.T., Haegeman, A., Danchin, E.G.J., Gaur, H.S., Helder, J., Jones, M.G.K., Kikuchi, T., Manzanilla-López, R., Palomares-Rius, J.E., Wesemael, W.M.L., Perry, R.N., 2013. Top 10 plant-parasitic nematodes in molecular plant pathology. Molecular Plant Pathology 14, 946–961. doi:10.1111/mpp.12057.

Jones, J.W., Hoogenboom, G., Porter, C.H., Boote, K.J., Batchelor, W.D., Hunt, L.A., Wilkens, P.W., Singh, U., Gijsman, A.J., Ritchie, J.T., 2003. The DSSAT cropping system model. European Journal of Agronomy 3, 235–265. doi:10.1016/S1161-0301(02)00107-7.

Joshi, V., Kumar, S., Rawat, S., 2020. Study on infection and development of root-knot nematode, Meloidogyne javanica on mungbean. Journal of Entomology and Zoology Studies .

Kropff, M.J., Teng, P.S., Rabbinge, R., 1995. The challenge of linking pest and crop models. Agricultural Systems 49, 413–434. doi:10.1016/0308-521X(95)00034-3.

Lamboni, M., Makowski, D., Lehuger, S., Gabrielle, B., Monod, H., 2009. Multivariate global sensitivity analysis for dynamic crop models. Field Crops Research 113, 312–320. doi:10.1016/j.fcr.2009.06.007.

Lamboni, M., Monod, H., Makowski, D., 2011. Multivariate sensitivity analysis to measure global contribution of input factors in dynamic models. Reliability Engineering & System Safety 96, 450–459. doi:10.1016/j.ress.2010.12.002.

Le Maitre, D.C., Midgley, J.J., 1991. Allometric relationships between leaf and inflorescence mass in the genus protea (proteaceae): an analysis of the exceptions to the rule. Functional Ecology 5, 476–484. doi:10.2307/2389629.

Li, L., 2007. Carbon concentration and its characteristics in terrestrial higher plants. Chinese Journal of Ecology .

Liu, H.F., Génard, M., Guichard, S., Bertin, N., 2007. Model-assisted analysis of tomato fruit growth in relation to carbon and water fluxes. Journal of Experimental Botany 58, 3567–3580. doi:10.1093/jxb/erm202.

Masri, S.F., Bekey, G.A., Safford, F.B., 1980. A global optimization algorithm using adaptive random search. Applied Mathematics and Computation 7, 353–375. doi:10.1016/0096-3003(80)90027-2.

Meher, H.C., Gajbhiye, V.T., Chawla, G., Singh, G., 2009. Virulence development and genetic polymorphism in *Meloidogyne incognita* (kofoid & white) chitwood after prolonged exposure to sublethal concentrations of nematicides and continuous growing of resistant tomato cultivars. Pest Management Science 65, 1201–1207. doi:10.1002/ps.1810.

Mekete, T., Mandefro, M., Greco, N., 2003. Relationship between initial population densities of Meloidogyne javanica and damage to pepper and tomato in Ethiopia. Nematologia Mediterranea .

Minchin, P.E.H., Thorpe, M.R., Farrar, J.F., 1993. A simple mechanistic model of phloem transport which explains sink priority. Journal of Experimental Botany 44, 947–955. doi:10.1093/jxb/44.5.947.

Moens, M., Perry, R.N., Starr, J.L., 2009. Meloidogyne species - a diverse group of novel and important plant parasites., in: Root-knot nematodes. CABI Books, pp. 1–17. doi:10.1079/9781845934927.0001.

Mu, X., Chen, Y., 2021. The physiological response of photosynthesis to nitrogen deficiency. Plant Physiology and Biochemistry 158, 76–82. doi:10.1016/j.plaphy.2020.11.019.

Nelder, J.A., Mead, R., 1965. A simplex method for function minimization. The Computer Journal 7, 308–313. doi:10.1093/comjnl/7.4.308.

Ney, B., Bancal, M.O., Bancal, P., Bingham, I.J., Foulkes, J., Gouache, D., Paveley, N., Smith, J., 2013. Crop architecture and crop tolerance to fungal diseases and insect herbivory. mechanisms to limit crop losses. European Journal of Plant Pathology 135, 561–580. doi:10.1007/s10658-012-0125-z.

Nilusmas, S., Mercat, M., Perrot, T., Djian-Caporalino, C., Castagnone-Sereno, P., Touzeau, S., Calcagno, V., Mailleret, L., 2020. Multi-seasonal modelling of plant-nematode interactions reveals efficient plant resistance deployment strategies. Evolutionary Applications 13, 2206–2221. doi:10.1111/eva.12989.

Ornat, C., Verdejo-Lucas, S., Sorribas, F.J., 2001. A population of meloidogyne javanica in spain virulent to the *Mi* resistance gene in tomato. Plant Disease 85, 271–276. doi:10.1094/PDIS.2001.85.3.271. publisher: Scientific Societies.

Penlap Tamagoua, J.J., Grognard, F., Baldazzi, V., Touzeau, S., 2025. Plant tolerance is explained by resource-based plant–nematode interactions. URL: https://inria.hal.science/hal-05394092. HAL preprint.

Pineda, O., Bonierbale, M.W., Plaisted, R.L., Brodie, B.B., Tanksley, S.D., 1993. Identification of *RFLP* markers linked to the *H1* gene conferring resistance to the potato cyst nematode *Globodera* rostochiensis. Genome 36, 152–156. doi:10.1139/g93-019.

Poorter, H., Niklas, K.J., Reich, P.B., Oleksyn, J., Poot, P., Mommer, L., 2012. Biomass allocation to leaves, stems and roots: meta-analyses of interspecific variation and environmental control. New Phytologist 193, 30–50. doi:10.1111/j.1469-8137.2011.03952.x.

Ralmi, N.H.A.A., Khandaker, M.M., Mat, N., 2016. Occurrence and control of root knot nematode in crops: a review. Australian Journal of Crop Science 10, 1649–1654. doi:10.21475/ajcs.2016.10.12.p7444.

Rice, D.C.J., Carriveau, R., Ting, D.S.K., Bata, M.H., 2017. Evaluation of crop to crop water demand forecasting: tomatoes and bell peppers grown in a commercial greenhouse. Agriculture 7, 104. doi:10.3390/agriculture7120104.

Sasser, J., 1979. Economic importance of *Meloidogyne* in tropical countries. Economic importance of Meloidogyne in tropical countries .

Sato, K., Kadota, Y., Shirasu, K., 2019. Plant immune responses to parasitic nematodes. Frontiers in Plant Science 10, 1165. doi:10.3389/fpls.2019.01165.

Shepherd, R.L., Huck, M.G., 1989. Progression of root-knot nematode symptoms and infection on resistant and susceptible cottons. Journal of Nematology 21, 235–241.

Sikora, R.A., Coyne, D.L., Hallmann, J., Timper, P., 2018. Plant parasitic nematodes in subtropical and tropical agriculture. CAB International.

Snyder, D.W., Opperman, C.H., Bird, D.M., 2006. A method for generating *Meloidogyne incognita* males. Journal of nematology 38, 192–194.

Spiegel, Y., Cohn, E., Kafkafi, U., Sulami, M., 1982. Influence of potassium and nitrogen fertilization on parasitism by the root-knot nematode *Meloidogyne javanica*. Journal of Nematology 14, 530.

Steduto, P., Hsiao, T.C., Raes, D., Fereres, E., 2009. Aquacrop - the fao crop model to simulate yield response to water: concepts and underlying principles. Agronomy Journal 101, 426–437. doi:10.2134/agronj2008.0139s.

Stöckle, C.O., Donatelli, M., Nelson, R., 2003. CropSyst, a cropping systems simulation model. European Journal of Agronomy , 289–307doi:10.1016/S1161-0301(02)00109-0.

Subbotin, S.A., Palomares Rius, J.E., Castillo, P., 2021. Systematics of root-knot nematodes (nematoda: Meloidogynidae), in: Nematology Monographs and Perspectives, BRILL. p. 872. doi:10.1163/9789004387584.

Subedi, S., Thapa, B., Shrestha, J., 2020. Root-knot nematode (*Meloidogyne incognita*) and its management: a review. Journal of Agriculture and Natural Resources 3, 21–31. doi:10.3126/janr.v3i2.32298.

Tankam-Chedjou, I., Touzeau, S., Mailleret, L., Tewa, J.J., Grognard, F., 2020. Modelling and control of a banana soilborne pest in a multi-seasonal framework. Mathematical Biosciences 322, 108324. doi:10.1016/j.mbs.2020.108324.

Thornley, J., 1996. Modelling water in crops and plant ecosystems. Annals of Botany 77, 261–275. doi:10.1006/anbo.1996.0030.

Thornley, J.H.M., 1972. A model to describe the partitioning of photosynthate during vegetative plant growth. Annals of Botany 36, 419–430. doi:10.1093/oxfordjournals.aob.a084601.

Thornley, J.H.M., Cannell, M.G.R., 2000. Modelling the components of plant respiration: representation and realism. Annals of Botany 85, 55–67. doi:10.1006/anbo.1999.0997.

Thornley, J.H.M., Johnson, I.R., 1990. Plant and Crop Modelling: A Mathematical Approach to Plant and Crop Physiology. 1 ed., Clarendon Press, Oxford, Oxford, UK.

Tixier, P., Risède, J.M., Dorel, M., Malézieux, E., 2006. Modelling population dynamics of banana plant-parasitic nematodes: A contribution to the design of sustainable cropping systems. Ecological Modelling 198, 321–331. doi:10.1016/j.ecolmodel.2006.05.003.

Tomczak, A., Koropacka, K., Smant, G., Goverse, A., Bakker, E., 2009. Resistant plant responses, in: Berg, R.H., Taylor, C.G. (Eds.), Cell Biology of Plant Nematode Parasitism, Springer Berlin Heidelberg, Berlin, Heidelberg. pp. 83–113. doi:10.1007/978-3-540-85215-5_4.

Trudgill, D.L., Cotes, L.M., 1983. Tolerance of potato to potato cyst nematodes (*Globodera rostochiensis and G. pallida*) in relation to the growth and efficiency of the root system. Annals of Applied Biology 102, 385–397. doi:10.1111/j.1744-7348.1983.tb02708.x.

Wallace, H., 1987. A perception of tolerance. Nematologica 33, 419–432. doi:10.1163/187529287X00083.

Wang, Y., Jing, T., Liu, X., Ai, X., Bi, H., 2024. Sltdc modulates photosynthesis of senescent leaves in tomato. Horticulture Advances 2, 16. doi:10.1007/s44281-024-00039-2.

Weng, J.H., 2000. The role of active and passive water uptake in maintaining leaf water status and photosynthesis in tomato under water deficit. Plant Production Science 3, 296–298. doi:10.1626/pps.3.296.

Wilkes, J.E., Kirkpatrick, T.L., 2020. The effects of and on the yield and quality of edamame in arkansas. Journal of Nematology 52, 1–15. doi:10.21307/jofnem-2020-012.

Williamson, V.M., Hussey, R.S., 1996. Nematode pathogenesis and resistance in plants. The Plant Cell 8, 1735–1745. doi:10.1105/tpc.8.10.1735.

Wise, M.J., Abrahamson, W.G., 2005. Beyond the compensatory continuum: environmental resource levels and plant tolerance of herbivory. Oikos 109, 417–428. doi:10.1111/j.0030-1299.2005.13878.x.

Yadav, S., Kumar, V., 2022. A prey–predator model and control of a nematodes pest using control in banana: mathematical modeling and qualitative analysis. International Journal of Biomathematics 15, 2150089. doi:10.1142/S1793524521500893.

Zaffaroni, M., Cunniffe, N.J., Bevacqua, D., 2020. An ecophysiological model of plant–pest interactions: the role of nutrient and water availability. Journal of The Royal Society Interface 17. doi:10.1098/rsif.2020.0356.

1184 Zeck, W.M., 1971. A rating scheme for field evaluation of root-knot nematode infestations.
1185 Pflanzenschutz-Nachrichten Bayer , 141–144.

1186 Zeinali, E., Soltani, A., Toorani, M., Khadempir, M., 2014. Allometric relationships between leaf
1187 area and vegetative characteristics in faba bean (Vicia faba L.). Journal of Plant Production
1188 Research 20, 1–22.